AN ABSTRACT OF THE THESIS OF

Jack A. Puleo for the degree of Master of Science in Oceanography presented on July 14, 1998. Title: Swash Zone Sediment Suspension and Transport.

Redacted for privacy

Abstract approved: _____
Robert A. Holman

Redacted for privacy

John S. Allen

Swash zone processes are of significant importance to foreshore morphologic change. This thesis addresses the importance of the uprush and backwash fluid motions and flow duration effects to the resulting sediment transport. The analysis relates the field observations to well known sediment transport formulations as well as investigates the importance of bore generated turbulence.

The field study was conducted at Gleneden Beach, OR during February 25-28, 1994. Data were collected by continuously monitoring suspended sediment concentrations (SSC), sea surface elevations, and velocity (z=4 and 8 cm) at 3 cross-shore locations within the swash zone spanning high tides. SSC and bed level fluctuations were monitored using a vertical stack of Fiber optic Optical Backscatter Sensors (FOBS) which penetrated the bed. Foreshore surveys and video run-up data were also collected.

Results showed that the uprush suspension was high, concentrated in the leading edge and nearly vertically uniform over the water column. Shortly after the sensors were inundated by runup, the sediment rapidly settled out of the water column as observed at the sensor location. The observed settling was in part due to advection of the sediment laden uprush migrating passed the sensor. Through flow reversal, the SSC was small. SSC increased again in the backwash although vertical profiles were markedly different from uprush profiles with much of the suspension being confined to very near the bed where strong vertical gradients in SSC existed. The amount of backwash suspension appeared to be affected by flow duration.

Suspended load transport comparisons with Bagnold-type energetics formulations did not yield strong relationships for instantaneous transport or total uprush or backwash transport. Suspended sediment transport in the leading edge of swash zone bores showed some dependence on the estimated energy dissipation across the bore front.

The field observations and analysis supported the following uprush scenario: A surf zone bore migrates into shallow water and begins to influence local sediment transport processes, until the water depth in front of the bore approaches zero causing the bore to collapse. Bore turbulence and bore collapse dissipate energy, which may maintain sediment in suspension. The suspended sediment is advected with the uprush front as it travels up the beach face, but the ability to maintain the sediment in suspension decreases causing the sediment to settle out of the water column. near flow reversal.

Swash Zone Sediment Suspension and Transport

by

Jack A. Puleo

A THESIS

submitted to

Oregon State University

in partial fulfillment of
the requirements for the
degree of

Master of Science

Presented July 14, 1998
Commencement June 1999

Master of Science thesis of Jack A. Puleo presented on July 14, 1998

APPROVED:

Redacted for privacy

Co-major professor, representing Oceanography

Redacted for privacy

Co-major professor, representing Oceanography

Redacted for privacy

Dean of the College of Oceanic and Atmospheric Sciences

Redacted for privacy

Dean of Graduate School

I understand that my thesis will become part of the permanent collection of Oregon State University libraries. My signature below authorizes release of my thesis to any reader upon request.

Redacted for privacy

Jack A. Puleo, Author

ACKNOWLEDGEMENTS

My time at OSU has been a very fruitful one. My undergraduate education had given me a firm foundation for what I was to face during the rigors of graduate school. However, my education was far from complete. Thankfully, I learned more than most could hope for from the excellent faculty and resources here. Upon arriving, I was given a unique data set to analyze and yet I had no clue about data analysis or even how to use the visualization software that was to aid in my analysis. What was shocking was that this was the first time I was given data and not told what to do with it. All through my undergraduate years I performed many small projects each of which had an obvious task with which to compare this to that. It was here that I truly learned to use my brain to try new things and to look at science from a different viewpoint. I owe much of this insight to Rob Holman and Reg Beach who I initially worked with. Rob and Reg both taught me a new way of thinking and would not let me settle on ideas that had already been published or thought up. I am also grateful to Rob for serving as my chief advisor, for helping to get me accepted at OSU and for eventually suggesting that I become part of the Coastal Imaging Lab.

My stay here has had me searching out a variety of scientists to answer many questions. I would like to extend my thanks to John Allen for accepting me as his student and serving as an advisor in my research and on my committee. John has a mathematical way about him that I doubt I will ever see in other scientists. It took me a while but I am a little more proficient at speaking his language (mathematics). He was especially helpful in the derivations and understanding process in the latter portions of this thesis

work. Other thanks are extended to Ron Guenther, Murray Levine, Charles Sollitt, Dudley Chelton, Paul Komar, Todd Holland and Casey Church.

Now for the Coastal Imaging Lab. My time here was made all that much better by being surrounded by such great people. "Who wants to talk swash?" This is a phrase I bet all of you will be happy to never hear again. John and Steve did an excellent job with the computers and data and handled my continual barrage of questions as well as my weekly (sometimes daily) computer screw-ups (anyone killed robijn lately?). Bill was a great friend this last year and helped me get through some tough classes. Nathaniel provided many thought provoking answers to questions that I was not sure I asked but somehow what he said eventually made sense. Kathy was a great roommate and fun to have around the lab. Babs, the 'ultimate' all-star, always had the energy to get me out of the office and onto the field (except during the last few months) or to find the nearest party.

As the length of these acknowledgements grows, I feel I had better sum up by thanking the people outside the science world that have made my life complete. Of course, this begins with my family. My brothers (Corey and Nick), sisters (Lisa and Patty) and nieces and nephews (Jana, Alex, Jess and Andrew) have been nothing but supportive and a joy to be around. Lilcs, my love, has stuck it out with me through my extremely crazy times when I could think of nothing but work. Now, there is much to show for it as we begin our married future together. Tom, my best bud, has been there through some tough times, and made my life since through high school to the present all the more interesting. I doubt I will ever find another friend of this caliber wherever my

career takes me. Finally, I have to thank two of the best parents (Anna and Russ Puleo) any child could ask for. They always pushed me to do the right things, but never so hard that I despised them for it. In fact, I have my father to thank for indirectly acquainting me with oceanography. When I was younger, he often took me to the aquarium or to the jetties to fish or swim. It was these first trips to the ocean that piqued my interest in oceanography and allowed me to decide at a young age that I was going to grow up studying the ocean. It is because of their love and support that I am dedicating this thesis to my parents.

CONTRIBUTION OF AUTHORS

Dr. Reggie Beach was involved in the preliminary analysis, reviews of this manuscript as well as setting up and conducting the field experiment with Dr. Rob Holman. Dr. Holman aided in the analysis, writing and reviewing of many drafts. Dr. John Allen assisted in the development of the section pertaining to bore dissipation and mass and momentum conservation as well as assisting in draft reviews.

TABLE OF CONTENTS

TABLE OF CONTENTS (Continued)

LIST OF FIGURES

LIST OF FIGURES (Continued)

LIST OF TABLES

LIST OF SYMBOLS

Symbol	
α	Sediment solidity (=1-sediment porosity)
β	Beach angle of elevation
δt	Data recording interval
ε_b	Bedload efficiency factor
ε_s	Suspended load efficiency factor
ϕ	Internal friction angle of sediment
η	Water depth
ρ	Fluid density
ρ_s	Sediment density
τ_o	Bed shear stress
ω	Fluid power
ζ	Depth of integration for suspended load calculations
c	Suspended sediment concentration
C	Suspended load
f	Friction factor for quadratic stress law
Fr	Froude number $u/(gh)^{1/2}$
g	Gravitational acceleration
h	Water depth for bore calculations
i	Observed instantaneous immersed weight sediment transport rate

LIST OF SYMBOLS (Continued)

Symbol	
i^*	Mean observed immersed weight sediment transport rate across the bore
I	Observed total immersed weight sediment transport
j	Mass flux per unit volume (ρuh)
P	Hydrostatic pressure
PE	Time rate of change of potential energy of sediment
q	Energy flux density per unit width per unit time
Q	Sediment flux
s	immersed weight ratio, $(\rho_s-\rho)/\rho_s$
u	general notation for cross-shore velocity
$\bar{u}$	general notation for mean cross-shore velocity
u'	Water particle velocity
U_b	Bore velocity
$\bar{U}_s$	Suspended sediment particle velocity
u_1	Flow velocity on low (supercritical) side of bore in frame of reference of bore
u_2	Flow velocity on high (subcritical) side of bore in frame of reference of bore
U1	Cross-shore velocity from lower current meter in time series
U2	Cross-shore velocity from upper current meter in time series
w	Sediment fall velocity
W	Predicted instantaneous immersed weight sediment transport rate for suspended load

LIST OF SYMBOLS (Continued)

Symbol

W^*	Mean predicted immersed weight sediment transport rate
W_b	Predicted instantaneous immersed weight sediment transport rate for bed load

SWASH ZONE SEDIMENT SUSPENSION AND TRANSPORT

CHAPTER ONE: GENERAL INTRODUCTION

Swash zone

As deep water waves propagate into the near-shore region (Figure 1.1) and begin to "feel" bottom, the orbital motions can begin to affect the sea bed. As the waves travel further shoreward, they reach a depth where they begin to break. The turbulence associated with wave breaking can be an important sediment entraining mechanism if the waves break in water shallow enough to enable the turbulence to reach the bed. Following breaking, a bore forms and travels across the surf zone continually dissipating energy. Eventually, the bore may reach the beach face where it becomes swash. The swash zone represents another area of the nearshore where turbulence may become an important sediment entraining and/or transporting mechanism. The circles in Figure 1.1 represent an instrument that may be placed *in situ* to measure properties such as velocity, water depth or suspended sediment concentrations. It is clear from the diagram that the 2 instruments on the left side will be continually submerged while the instrument to the right (the one within the swash zone) may only be sporadically inundated, which complicates data analysis.

The definition of the swash zone is that region of the beach that is alternately wet or dry due to the action of the wave run-up. Figure 1.2 shows a conceptual time history

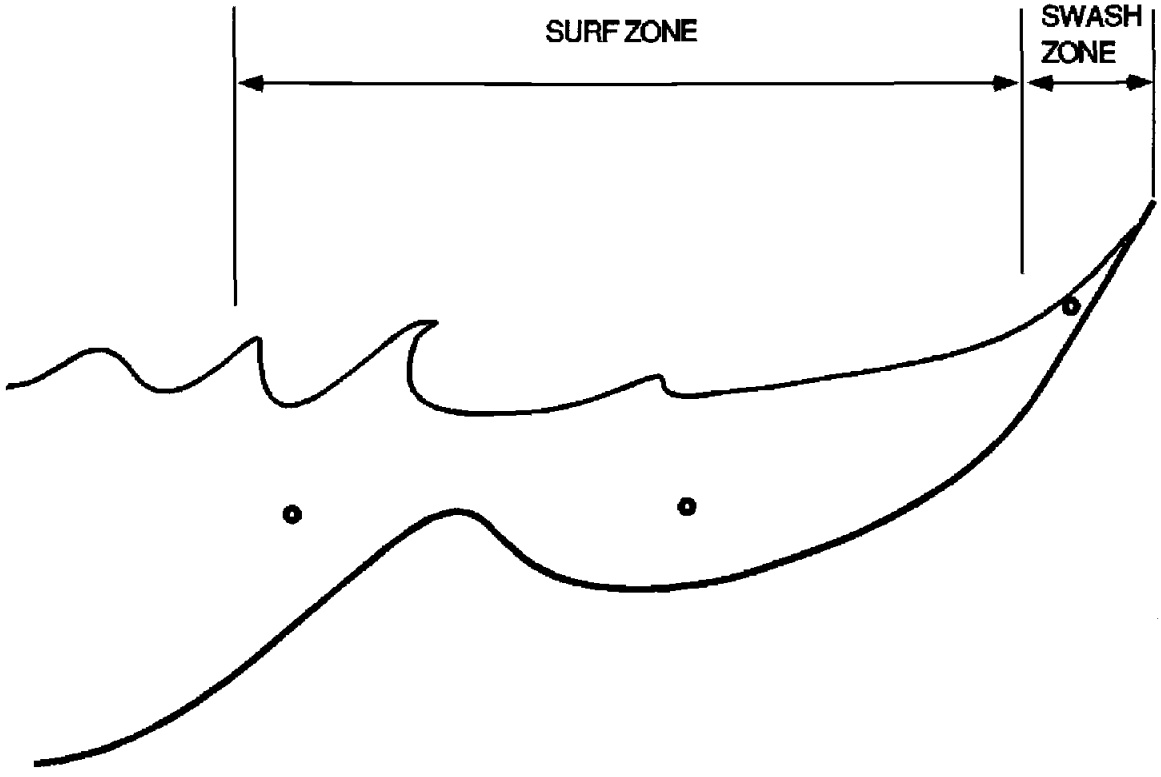

Figure 1.1. Schematic of nearshore showing shoaling waves, breaking, surf zone bores and run-up in the swash zone. Circles in the figure represent an instrument that may be placed *in situ* to measure a property such as velocity or sea surface elevation.

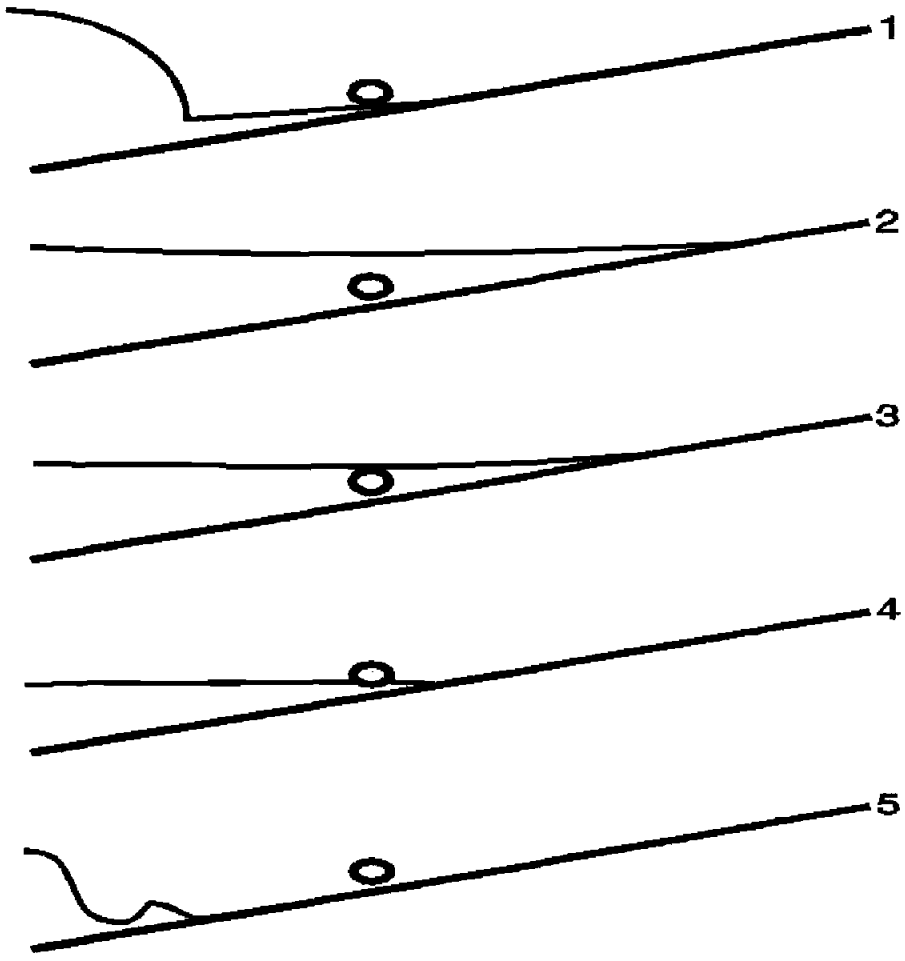

Figure 1.2. Conceptual time history of swash motions. The circle represents an *in situ* instrument placed above the beach (sloped line). At time 1 a bore has migrated into very shallow water. By time 2 it has collapsed and started the swash run-up process and reached a zero velocity or flow reversal. Times 4 and 5 show the backwash as the water mass moves downslope under the force of gravity. The backwash has collided with the next uprush at Time 5.

of a swash cycle. The straight line represents the beach face, while the bold line represents the sea surface. Circles represent an instrument that may be deployed in this region to measure some property such as water depth or velocity. At time 1, a bore has migrated into the swash zone over water of very shallow depth. When the bore reaches the initial shoreline (the intersection of the water level and the beach at time 1), the bore is said to collapse and the run-up process begins (Figure 1.2; time 2). The run-up moves up the beach face as a continually thinning mass of water (Figure 1.2; time 3). Eventually the velocity slows to zero and the water begins to move seaward under the force of gravity (Figure 1.2; time 4). Because there is a continuous train of bores migrating into the swash zone, the backwash will be met by the next uprush and a violent turbulent collision may take place before the next uprush begins (Figure 1.2; time 5). The collision process may be an important mechanism to sediment transport (discussed shortly). From the conceptual time history of the swash cycle, it seems likely that the fluid motions within the backwash may not simply be the reverse of the uprush.

Surf zone/swash zone comparison

From Figure 1.1 it was evident that instruments placed in the swash may not be continually inundated. This implies that a times series collected in the swash zone may be discontinuous and standard statistical procedures are often difficult to perform on these discontinuous time series. The discontinuity in swash time series versus surf zone time series is one example among many of the differences between the surf zone and the swash zone.

Some basic definitions that are used within the surf zone such as wavelength (distance between crests) and wave period (time for wave to travel one wavelength) do not have a simple mapping into the swash zone. For instance, one may define the beginning of an uprush as that time when the bore reaches the shoreline (Figure 1.2) and the end of the backwash as the time just before the next uprush begins. Conceptually these make sense, but due to the interactions of a random (natural) wave field, the time between these occurrences is not as constant as a peak period that may be observed in the surf zone. Hence the observed swash period for any individual swash cannot be assumed representative for a series of swash motions on a natural beach. Since the period of the swash motion will not be constant over time, we would not expect the swash wavelength to have constant (or roughly so) values either. Indeed, even defining the spatial location of the swash zone is difficult as it migrates across the beach face in response to tidal changes as well as responding to individual waves and wave trains. This latter notion suggests that the swash zone is a Lagrangian region of the nearshore. Within the swash zone, water is actually being advected up and down the beach face and so it would be more appropriate to follow individual water parcels as they move across the foreshore. This type of analysis, however, is not possible with fixed instrumentation.

Sediment transport

The swash zone has been shown in the past to be important in terms of beach erosion or accretion. Indeed, the swash zone *is* the region of shoreline erosion or accretion. Hence, this region becomes very important for recreation as well as for

developers and there is a need to understand how sediment suspension and transport occurs in the swash zone. Although the importance of the swash zone is widely recognized, relatively few studies have been performed when compared to the variety and abundance of surf zone studies. Specifically, few studies have reported sediment transport, flow velocities and water depths simultaneously which comprise the measurements that would be needed to model swash zone transport.

There are 2 main types of sediment transport that can exist in a given flow: suspended load and bed load. Suspended load is transported in the water column and supported by turbulent motions that can overcome the tendency for particles to settle under gravity. The bed load is the sediment that moves very close to the bed (often defined as sediment motion within 10 grain diameters of the bed) and is supported by inter-granular collisions. There is still a debate among the scientific community as to whether sediment transport in the swash zone is dominated by suspended load or bedload (see Horn and Mason, 1994). However, swash zone transport is generally assumed to be dominated by bedload. It is therefore, necessary to establish the importance (if any) of suspended load to improve our ability to predict swash zone transport.

To date, most sediment transport models relate the time-averaged transport to the velocity to some power (generally cubed). This concept arises from energetics arguments (Bagnold, 1963, 1966) that were originally developed for steady river flow and may not be appropriate for the unsteady flow in the swash zone. Furthermore, in these formulations, the turbulence to support sediment suspension is a direct result of shear

stresses at the bed. In steady river flow, or even in oscillatory flow with a well developed boundary layer, this seems appropriate. However, because the swash zone can be dominated by turbulence that is associated with a bore rather than that generated by bed shear, it seems likely that suspension and transport mechanisms may be systematically different in this region.

Objectives

The primary objectives of this thesis are two-fold. First the variations of sediment suspension and transport (temporally and spatially) within the swash zone will be documented. The sediment suspension and transport in uprush/backwash flows as well as relationships to flow duration will be addressed. Second, energy considerations for bore propagation will be analyzed in terms of dissipation. These dissipation rates will be compared to dissipation due to bed shear stress to obtain their importance to sediment transport.

These objectives are addressed in Chapter Two, titled "Observations of swash zone sediment suspension and transport on a steep beach: Variations between the uprush and backwash and the importance of bore generated turbulence" co-authored by Dr. Rob Holman, Dr. Reggie Beach and Dr. John Allen. A condensed version of this chapter will be submitted to the *Journal of Geophysical Research*. We present unique sediment suspension and velocity data from the swash zone in this chapter. It will be shown that suspension transport is substantial (not negligible as often assumed in transport models),

and is highly variable within a swash cycle. We will also analyze the importance of swash duration to sediment suspension as well as temporal and spatial variations in sediment suspension across the swash zone. Transport observations will be compared to commonly used energetics formulations. Bore turbulence and formulas for quantifying energy dissipation in a bore will be addressed so that transport observations can be compared to this dissipation.

CHAPTER TWO:

OBSERVATIONS OF SWASH ZONE SEDIMENT SUSPENSION AND TRANSPORT ON A STEEP BEACH: VARIATIONS BETWEEN THE UPRUSH AND BACKWASH AND THE IMPORTANCE OF BORE-GENERATED TURBULENCE

Abstract

A study of swash zone sediment transport was conducted at Gleneden Beach, OR during February 25-28, 1994. Data were collected by continuously monitoring suspended sediment concentrations (SSC), sea surface elevations, and velocity (z=4 and 8 cm) at 3 cross-shore locations within the swash zone spanning high tides. SSC and bed level fluctuations were monitored using a vertical stack of Fiber optic Optical Backscatter Sensors (FOBS) which penetrated the bed. Foreshore surveys and video run-up data were also collected. Ensemble averages of 6, 9, and 12 second duration swash events showed that the uprush suspension was high, concentrated in the leading edge and nearly vertically uniform above the lower 1-2 cm of the water column. Shortly after the sensors were inundated by runup, the sediment rapidly settled out of the water column as observed at the sensor location. The observed settling was in part due to advection of the sediment laden uprush migrating passed the sensor. During flow reversal, the SSC was small. SSC increased again in the backwash although vertical profiles were markedly different from uprush profiles with much of the suspension being confined to very near the bed where strong vertical gradients in SSC existed. The amount of backwash

suspension appeared to be affected by flow duration as backwash SSC increased from the 6 to 9 to 12 second events.

At times, strong cross-shore gradients in SSC were observed between the landward and seaward sensors with the landward sensors experiencing more sediment suspension on average than the seaward sensors. These strong cross-shore gradients, coupled with our definition of the swash zone width, imply that the transition between surf and swash zone occurs in a short (5-10 m) cross-shore distance. Suspended load transport comparisons with Bagnold-type energetics formulations did not yield strong correlations for instantaneous transport or total uprush or backwash transport. Suspended sediment transport in the leading edge of swash zone bores showed some dependence on the estimated energy dissipation across the bore front.

Introduction

The nearshore is a region where intense fluid/sediment interactions cause sediment suspension and transport that continually reshape local morphology. These processes are particularly apparent under the breaking waves of the surf and in the swash zone.

The swash zone may be defined as the region of the foreshore that is intermittently wet or dry from the action of the runup while the surf zone is the region that extends further seaward to the location where waves begin to dissipate by depth-induced breaking. The swash zone experiences large variations in sea surface elevations (dry to >1 m), cross-shore velocities ($\pm$ 3 m s^{-1}), and suspended sediment concentrations (SSC, 0 to >160 g l^{-1}). The swash zone is important to the sediment budget of the nearshore because it is the region of shoreline erosion or accretion, and swash processes determine whether sediment is stored on the upper beach or is instead returned to the inner surf zone and potentially transported offshore. In this regard, the swash zone acts as a sediment conduit between the upper beach and the surf zone.

There are fundamental differences between the surf and swash zones. Within the surf zone, Eulerian measurements made with fixed instruments are continuous as waves progress passed the sensors. However, swash is by definition, Lagrangian. Fixed instruments in the swash will record discontinuous time series as they alternately submerge and re-emerge from the passing swashes. Simple concepts like wave period can become complicated by the fact that it is probably duration of fluid coverage, not

repeat time scale which most influences sediment transport. In addition, the location of the swash zone itself is not constant in space or time and hence fixed instruments record in various locations of the swash zone throughout a tidal cycle.

The surf zone may also differ from the swash zone in terms of the physics involved in sediment suspension and transport. Within the surf zone, wave orbital motions reaching the sea bed can set up a boundary layer where bed shear stresses cause turbulence that may maintain sediment in suspension (most likely near the bed). Then, any mean flow can transport the suspended sediment. As waves break, form bores and move shoreward, the violent turbulence associated with the bore itself may reach the sea bed. This turbulence, which differs in generation from shear turbulence may be an important suspension mechanism within the swash zone. In fact, a possible definition of the seaward boundary of the swash zone may be the region where the bore turbulence begins to significantly affect local processes of sediment transport.

Because a swash consists of 2 parts (uprush and backwash), analysis would be simplified if the backwash dynamics were simply the reverse of the uprush dynamics. However, this is not the case. Uprush occurs directly after final bore collapse at the shoreline and can be thought of as the transport of a water mass up the beach face. The leading edge of the turbulent uprush (collapsing bore) travelling over very shallow bed could be expected to entrain and/or carry high quantities of suspended sediment due to the associated high turbulence levels reaching the bed. Madsen and Svendsen (1983) and Svendsen and Madsen (1984) developed a theoretical model of turbulent bores and showed that the turbulence is concentrated in the leading edge of the bore and spreads

downwards, towards the bed. Furthermore, they reported that the boundary layer development in a bore is much weaker than the boundary layer development in a stationary hydraulic jump and the boundary layer will not be significant until far behind the bore front and hence not associated with the bore itself. Yeh and Ghazali (1995) analyzed bore collapse and showed that the turbulence is advected with the bore front and ultimately acts on the dry beach bed which may imply that the bore turbulence is important to local sediment transport processes.

As the leading edge uprush velocity decreases, the settling velocity of the particles should become more important and sediment suspension should decrease until the uprush terminates at a maximum shoreward excursion. After flow reversal, the mass of water thins in a fashion such that the leading edge does not retreat downslope until most of the water mass has moved seaward (Emery and Gale, 1951) and this backwash flow may become analogous to uni-directional flow down an incline. As such, one would expect a growing boundary layer downstream in the flow and the height of the boundary layer may become flow-duration dependent. So, as the gravity-driven flow continues to thin and increase in velocity, the increasing bottom stresses may be able to suspend sediment higher into the water column. Hence backwash sediment suspension and transport may be flow-duration dependent. Furthermore, backwash termination is often associated with bore collision where the flow may go through a hydraulic jump (transition from supercritical, $u^2>gh$, to subcritical, $u^2<gh$, where u is the cross-shore velocity, g is gravity, and h is water depth, Broome and Komar, 1979) altering sediment transport.

It is generally accepted that beach erosion occurs during large waves and storm events. However it is not the large waves themselves that cause erosion. Experiments on fairly dissipative beaches have shown that swash amplitudes at incident periods are usually depth-limited, hence they do not increase with an increase in incident band energy. By contrast, swash amplitudes at lower, infragravity (.003-.03 Hz) frequencies, increase approximately linearly with an increase in incident band energy (e.g. Holman, 1981; Guza and Thornton, 1982; Holman and Sallenger, 1986). Mechanisms for the generation of these infragravity motions include nonlinear transfers from offshore wave groups or through breaking patterns of a modulating surf zone. Carlson (1984), Mase (1988), and Mase (1995) showed that the overtaking and capturing of bores in the lower swash zone could also lead to low frequency swash oscillations.

Since large waves substantially increase the amount of infragravity energy in the swash zone and since large waves are generally associated with beach erosion, then it follows that sediment transport due to infragravity dominated swash may be erosive. The concept of infragravity dominated swash zones leading to erosion is consistent with the previous concept of the suspension and transport capabilities of the swash zone being flow-duration dependent.

The objectives of this chapter are to use field data from a swash zone sediment transport study on a high energy beach to address the importance of uprush and backwash sediment suspension and transport. Specifically, the temporal and spatial characteristics, as well as the vertical structure of sediment suspension within the swash zone will be

analyzed. This analysis will enable us to determine the quantity of sediment suspended in the leading edge of the uprush as well as the importance of flow duration to backwash sediment suspension. Energy arguments across the bore front will then be developed which will enable us to compare energy dissipation via shear stress in the boundary layer to energy dissipation across the bore. Lastly, we will analyze sediment transport data in light of a Bagnold-type formulation as well as comparing the observed sediment response to energy dissipation associated with bore turbulence.

The following section will introduce the Bagnold-type sediment transport formulations and the energy considerations across a bore front. The field study and swash zone instrumentation will then be described. The next section will display the results relating to uprush and backwash suspension and transport as well as compare observed sediment transport to Bagnold and turbulence relations. Our results will then be discussed in light of other swash zone studies. Concluding thoughts will be presented in the last section.

Sediment transport and bore relations

Bagnold-type formulations

After the seminal work of Bagnold (1963, 1966) many nearshore sediment transport models have followed his general energetics approach to sediment transport. A flow travelling over an erodable bed will expend some energy due to shear stresses on the

bed. If these shear stresses overcome the tendency for the grains to settle under gravity, then the grains will begin to 'bounce', roll, or saltate across the bottom. The Bagnold-type model hinges on the fluid power, ω, that can be delivered to the sediment from the fluid. The transport formula given for bedload is

$$W_b = \frac{\varepsilon_b \omega}{\tan\phi - \tan\beta}, \tag{II.1}$$

where W_b is the predicted instantaneous immersed weight transport rate per unit width of bedload, ε_b is an efficiency factor (i.e.; all the fluid power is not directly available to transport sediment), ϕ is the internal friction angle of the sediment, and β is the angle of the foreshore with the horizontal. In principal, ω, is often related to a shear stress-velocity product, $\tau_o * \bar{u}$, for a bed shear stress, τ_o, and mean velocity $\bar{u}$. Furthermore, τ_o is often related to a quadratic stress law

$$\tau_o = \frac{1}{2}\rho f \bar{u}|\bar{u}|, \tag{II.2}$$

where ρ is the fluid density and f a friction factor. When II.2 is substituted into II.1, the Bagnold relation becomes

$$W_b = \frac{0.5\varepsilon_b \rho f \bar{u}^2|\bar{u}|}{\tan\phi - \tan\beta}. \tag{II.3}$$

So, the bedload transport becomes a function of the velocity cubed.

Several papers have addressed swash transport in a Bagnold-type manner with mixed results. Hughes *et al.*, (1997) separated swashes into uprush and backwash components and measured the total load transport within uprush events on a steep beach using a sediment trap similar to 'streamer traps' and ducted impeller current meters and tested the data against a bedload-type equation. By looking at 30 uprush events, they showed that the transport fell on a fairly straight line (although no r^2 value was reported) in log-log space when plotted against

$$\frac{\overline{u}^3 \Delta t}{\tan\phi + \tan\beta}, \qquad \text{(II.4)}$$

where Δt was the flow duration. Note, the '+' sign arises in the denominator of (II.4) due to the upslope flow direction. Since the sediment transport scales with the velocity cubed, Hughes *et al.*, 1997 regressed the observed immersed weight transport onto the numerator of (II.4) as well as varying the power of the velocity. The r^2 value was 0.78 when plotted against $\overline{u}^3\Delta t$. However, the regression had an r^2 value of 0.80 when plotted against $\overline{u}^2\Delta t$. Hardisty *et al.*, (1984) also attempted to explain swash zone sediment transport via a Bagnold-type relation. Bedload from the uprush and backwash was collected in sediment traps (although it is not clear that they sampled only bedload), while the velocity was monitored with a swinging vane. Their dry weight transport data, when plotted against (II.4) with the appropriate sign in the denominator depending on flow direction, had an r value of 0.21 for the uprush. Although there was much scatter in their plots, both r values (r value for backwash was not reported) were over the 90 % significant level. Interestingly, their uprush slope coefficient was over a factor of 5 larger

than the slope coefficient obtained by Hughes *et al.*, (1997). Osborne and Rooker (1997) performed a similar analysis by comparing the instantaneous cross-shore transport rate to the third and fourth moment of the velocity and reported that the both relationships were well correlated although they did not present r^2 or significance statistics. Other researchers have also analyzed sediment transport or formulated models based on the u^3 or Bagnold-type approach (e.g.; Wilson *et al.*, 1995; Bailard and Inman, 1981).

The above equation was used to relate the total load of sediment measured to a bedload only equation. This may be the cause for the discrepancies in the coefficients obtained as well as the scatter seen in some of the data. Bagnold (1963, 1966) also described a suspended load sediment transport model which is very similar to (II.4) except that an auto-suspension criterion appears in the denominator as opposed to the friction angle

$$W = \frac{0.5\varepsilon_s(1-\varepsilon_b)\rho f\overline{u}^2|\overline{u}|}{(w/\overline{U}_s)-\tan\beta}, \qquad (\text{II}.5)$$

where W is the predicted instantaneous immersed weight suspended sediment transport rate per unit width, w is the sediment fall velocity, ε_s is a suspended load efficiency factor and $\overline{U}_s$ is the suspended sediment transport velocity. If it is assumed that $\overline{U}_s = \overline{u}$, then W is related to the velocity to the fourth power. The auto-suspension criterion (Bagnold, 1963, 1966; Seymour, 1986) arises if the beach slope is less than the fall velocity divided by the transport velocity. Put simply, it will take no extra energy from the flow to

transport the suspended sediment offshore as the resultant sediment motion approaches the slope of the beach. A turbidity current is a common example of an auto-suspending flow.

Bore relations and energy dissipation

In analyzing a fluid flow, it is often advantageous to develop non-dimensional parameters such that similarity can be obtained when comparing flows of different magnitudes (ie; Reynolds number). One such number that is often of importance to hydrologists in river flow is the Froude number, Fr, defined as the ratio of the flow velocity to gravitational forces or:

$$Fr = \frac{u}{\sqrt{gh}}, \tag{II.6}$$

where u is the flow velocity, h the water depth, g the gravitational acceleration and $(gh)^{1/2}$ the linear shallow water wave velocity. The importance of the Froude number is evident whenever a flow passes through the supercritical (Fr>1) to subcritical (Fr<1) stage, whence a hydraulic jump occurs (Fr=1). This can occur when a flow encounters a bathymetric anomaly (e.g. a ripple) and the associated surface waves cannot propagate in the upstream direction. Hence, a hydraulic jump can be thought of as a wave which moves upstream with a velocity $(gh)^{1/2}$ that is equivalent to the down stream velocity, u, such that the wave is stationary (Figure 2.1A; U_b=0). The turbulence associated with a

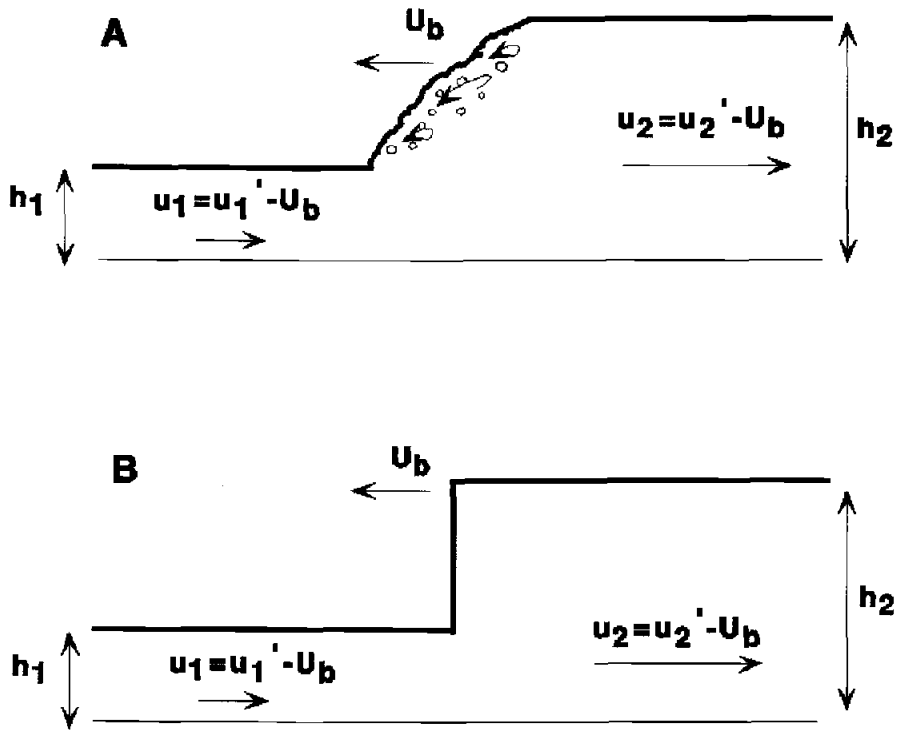

Figure 2.1. A) Schematic of hydraulic jump (U_b=0) or bore (U_b≠0), where U_b is the bore velocity. The subscripts 1 and 2 refer to the low side and high side of the bore or hydraulic jump respectively. The local water depth is h, u' is the particle velocity and u is the particle velocity in the frame of reference of the bore. B) Discontinuous representation as estimate of transition across the bore front.

hydraulic jump is an efficient energy dissipater and hence hydraulic jumps are commonly seen below dams and created in some channel flow by means of a stilling basin. The type of hydraulic jump can be dependent on the Froude number prior to the jump. Broome and Komar (1979), discussed undular jumps within the backwash that produced small wavelets and associated backwash ripples for initial Fr=2. If the initial Fr>4 then a fully turbulent jump will occur (Sellin, 1969) with an associated abrupt increase in water level. In either case, the hydraulic jump may be able to suspend sediment into the water column due to the associated turbulent eddies.

A turbulent bore can be thought of as a hydraulic jump (stationary) if it is observed in a coordinate system that is moving with the bore itself (Figure 2.1A; $U_b \neq 0$). The turbulence associated with a hydraulic jump or bore may be an important sediment suspending mechanism. In order to analyze any such relations, it is advantageous to determine the amount of energy dissipated across a bore. The Rankine-Hugoniot jump relations are (Johnson, 1997; Landau and Lifschitz, 1959)

$$u_1 h_1 = u_2 h_2 \tag{II.7}$$

$$u_1^2 h_1 + \frac{1}{2} g h_1^2 = u_2^2 h_2 + \frac{1}{2} g h_2^2, \tag{II.8}$$

where $u=u'-U_b$, U_b is the bore velocity, u' is the water particle velocity (assumed depth uniform), and h is the water depth. If $U_b=0$, then a stationary hydraulic jump exists. If

$U_b \neq 0$, then the equations describe a hydraulic jump in the frame of reference of the bore. The subscripts (1 and 2) denote the values on the low (supercritical) side and high (subcritical) side of the bore respectively (see Figure 2.1). Equation II.7 describes conservation of mass across the bore, while II.8 describes the conservation of momentum flux density, M, across the bore and is obtained by integrating $P+\rho u^2$ over the channel depth, where P is the hydrostatic pressure, ρgz, with ρ, the density, and z the vertical coordinate. Equations II.7 and II.8 will be useful to test our ability to conserve mass and momentum from the field data.

In principal, the bore (or hydraulic jump) is modeled as a discontinuity (Figure 2.1B). The energy fluxes on the two sides of the discontinuity will not be equal with their difference resulting from turbulent dissipation of energy across the discontinuity. The energy flux density per unit width, per unit time q, is (Landau and Lifschitz, 1959)

$$q = \int_0^h \left(\frac{P}{\rho} + \frac{1}{2} u^2 \right) \rho u dz = \frac{1}{2} j \left(gh + u^2 \right), \tag{II.9}$$

where $j=\rho uh$. Using II.8 and II.9 the difference (= energy dissipation) across the bore becomes

$$q_1 - q_2 = \frac{gj\left(h_1^2 + h_2^2\right)\left(h_2 - h_1\right)}{4h_1 h_2}. \tag{II.10}$$

Field Study

Study Site

Gleneden Beach is located on the central Oregon coast south of Siletz Spit in the Lincoln City Littoral Cell (Figure 2.2; Shih and Komar, 1994). The 24 km long littoral cell is bounded to the north by Cascade Head and to the south by the Government Point area of Cape Foulweather (Shih and Komar, 1994). The beach can be characterized as intermediate to steep with a beach face slope of roughly 1:12 and a mean sediment grain size of 440 microns obtained from samples near the instrumentation. Shih and Komar (1994), however have shown that the grain size distribution from this beach can be multimodal. During the experiment the wave approach was from the south. Significant wave heights recorded in 128 m depth off of Newport (15 km. S) by the CMAN buoy were 1.5 to 2.0 m with a peak period of 10 seconds over the duration of the run. Semi-diurnal tidal range on the Oregon coast is 2-3 m.

Instrumentation

The experiment utilized 3 instrument bars each consisting of a FOBS system (Fiber optic Optical Backscatter Sensor; Beach *et al.*, 1992a), two ducted-impeller current meters (Smith, 1978), and a pressure sensor (Figure 2.3). The FOBS was designed on the same principle as the Optical Backscatter Sensors (OBS; D & A Instruments)

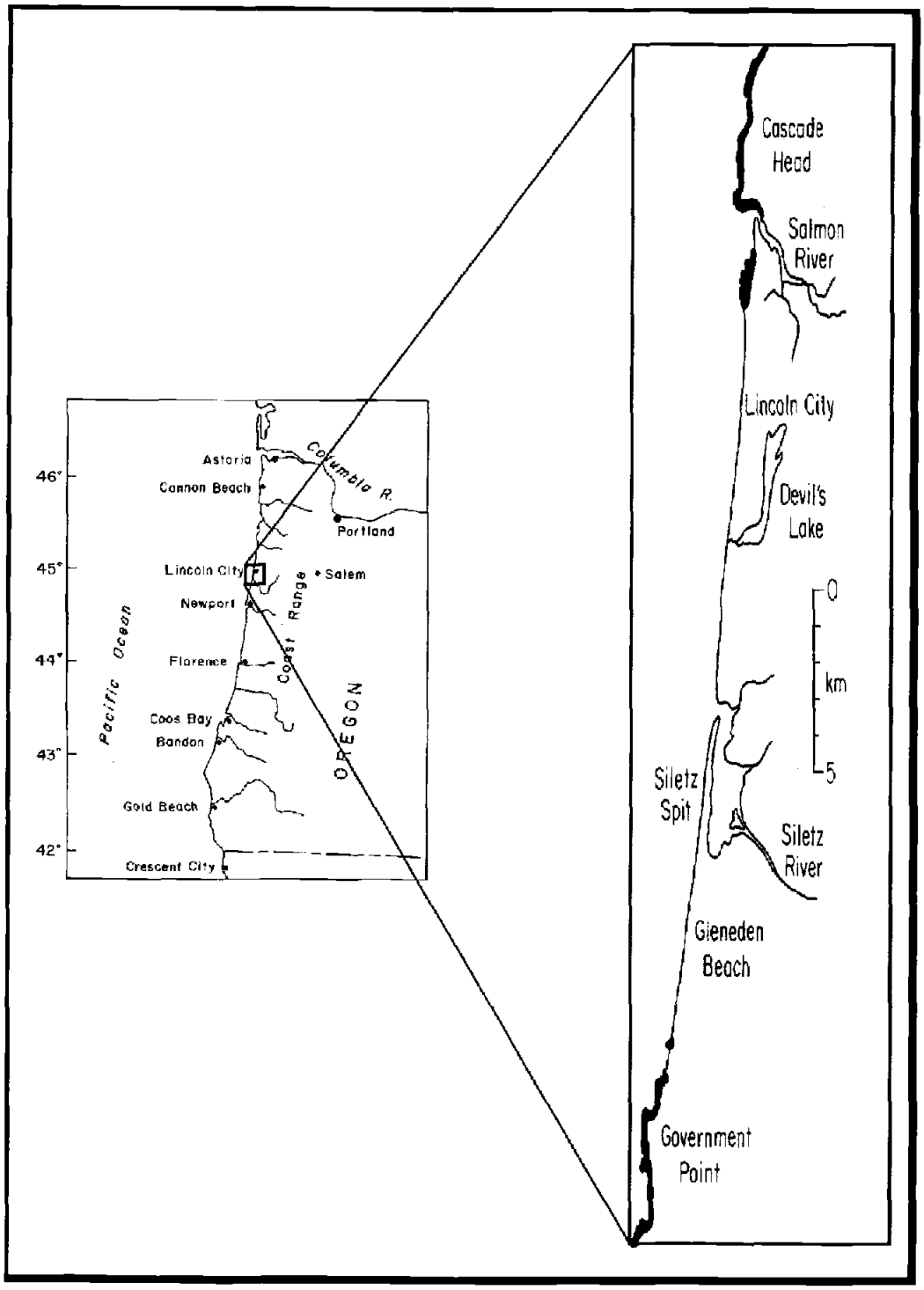

Figure 2.2. Location of field site within the Lincoln City Littoral Cell.

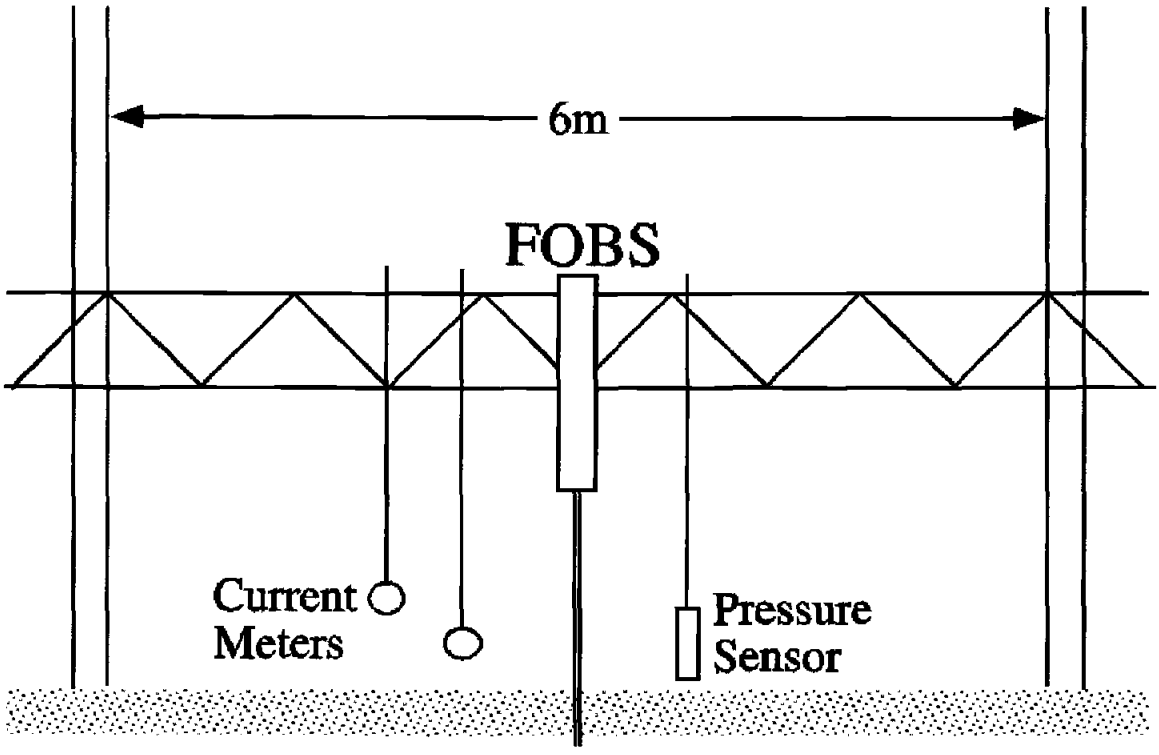

Figure 2.3. Diagram of instrument bar and instrumentation used in the study. The ducted impeller current meters were located at z=4cm and z=8 cm and the sensing portion of the pressure sensor at the bed initially. The lower 7 sensors of the FOBS array were initially buried.

but with a smaller size to allow for improved vertical resolution. These particular FOBS systems contain 19 sensor probe heads (~2.5 mm diameter; Figure 2.4), each consisting of 2 parallel fibers located in a common plane. One fiber acts as a light source while the other fiber measures the light backscattered from suspended particles. The sensor probe heads were arranged in a vertical array with spacings of 1 cm. For the most seaward site, the spacing was changed to 2 cm for the 9^{th} through 19^{th} sensor heads. The small diameter of the FOBS array allows for beach penetration without noticeable scour, yielding simultaneous measurements of bed level fluctuations as sensors were covered or uncovered by accretion or erosion. Because the optical properties of sediment vary with particle size and type, the FOBS sensors were calibrated in the laboratory in a recirculating tank using sediment collected from the swash zone at Gleneden Beach.

Field deployment

Each instrument bar consisted of a 6.1 m (20 ft.) long triangular radio antenna sections mounted between vertical pipes jetted into the beach face. Three instrument locations were deployed in the swash zone with cross-shore spacings of approximately 5 m (Figure 2.5). To reduce scour and wake effects, instruments were separated by 1-2 m in the alongshore direction from support pipes and all wiring was connected to the support pipes or was suspended above the instruments and out of the water column. All instruments were carefully collocated so that time varying elevations above the bed could be determined from the FOBS stack. The FOBS was initially oriented so that the lower 7

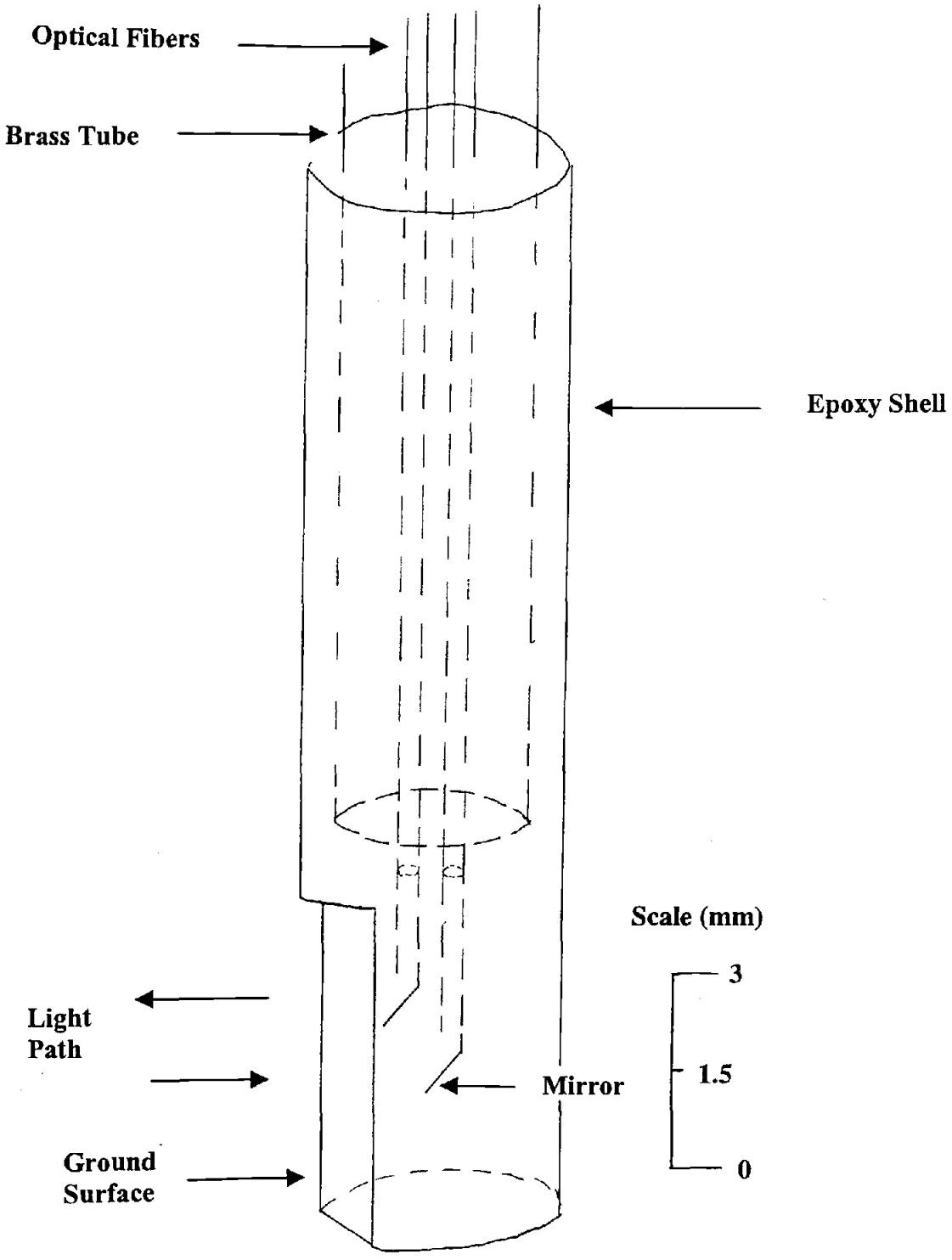

Figure 2.4. Sketch of FOBS probe head. The scale shows the size to be roughly 2.5 mm in diameter and 10 mm long.

Figure 2.5. Picture of field set up for swash zone study at Gleneden Beach. The three instrument bars in the cross-shore were separated by roughly 5 m. The video camera used to monitor the leading edge of the swash was located atop the tower in the left side of the figure.

sensors were buried. The ducted-impeller current meters were located at 4 and 8 cm above the bed while the sensing portion of the pressure sensor was located approximately at the bed at the beginning of the data run. Video cameras were used to monitor the run-up within the study region (Holland and Holman, 1997). Time stacks of the video data yielded a continuous time series for the leading edge of the swash.

Initial data analysis

Time series data

Data runs ranging from 30 minutes to approximately 4.5 hours were collected during February 25-28, 1994. Data were collected spanning high tide to reduce tidal effects, recorded at 16 Hz and later block averaged to 4 Hz. The data presented here, from February 27, 1994, combined the longest run with the best sampling execution, and are representative of the experiment.

Figure 2.6 is a representative 10 minute time series, at the landward location, of the sea surface elevation, cross-shore velocity at 2 locations above the bed, and suspended sediment concentrations at 7 locations in the vertical. The sea surface elevation, η, (Figure 2.6A) shows intermittent pulses corresponding to individual swash events separated by periods when the sensors are left completely dry. The signal variation of 0 to 80 cm displays the variable range of this region with even greater sea surface ranges occurring in other portions of the run. The velocity at the two locations, U1 and

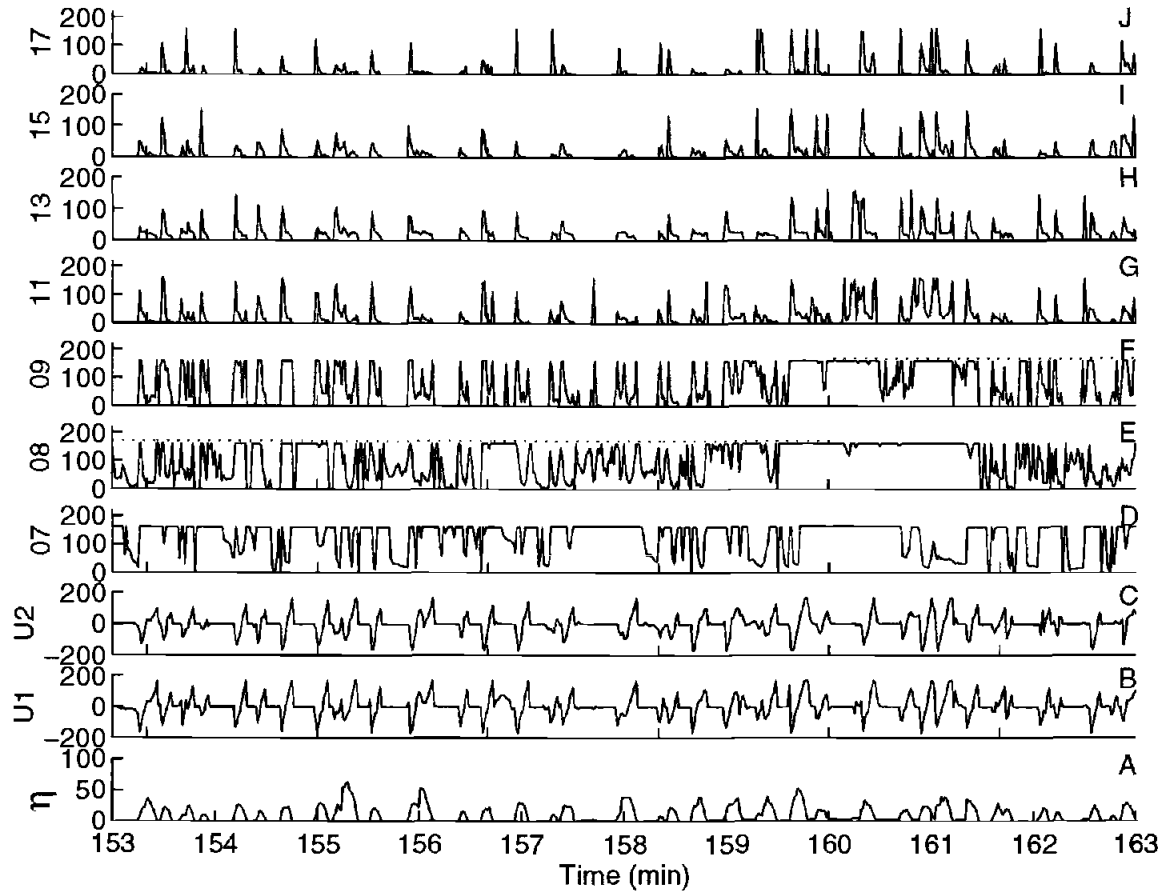

Figure 2.6. Ten minute time series from landward sensors. A) Sea surface elevation, η, (cm). B,C) Velocity, U1 at z=4 cm and U2 at z=8 cm above the bed (cm s^{-1}). D-J) Fobs output (g l^{-1}) The number on the y-axis corresponds to the sensor location in the vertical array (ex. CB07 is 7th sensors from bottom of array). The dotted lines in E,F correspond to location of the bed as determined from the bed level finding routine (discussed shortly).

U2, (Figure 2.6 B,C) first shows a nearly instantaneous negative pulse to a maximum onshore, followed by flow reversal, a positive pulse indicating an offshore flow or backwash and finally zero velocity as the sensor dries. Maximum cross-shore velocities can exceed 160 cm s^{-1} (maximum sensor output). Suspension events occur during the passage of the swash and can be seen to extend into the water column (Figure 2.6 D-J) with individual peaks in suspended sediment concentration exceeding 100 g l^{-1} at 11 cm above the bed. Quite often, each swash has an asymmetric two peaked suspension pulse corresponding to the uprush and backwash, with the uprush generally carrying more suspended sediment. The two velocity sensors appear highly correlated. The velocity time series will be used to choose various duration swash events (discussed later).

Run-up

A 2 minute video run-up times series of the leading edge of the swash is shown in Figure 2.7A. The dashed lines in the figure represent the cross-shore location of the 3 instrument bars, where 60 is the location of the landward instruments and 70 the location of the seaward instruments. Since landward is toward the top of the figure, the curve near 91 minutes shows the uprush motion of the leading edge, followed by flow reversal, and backwash termination approximately 8 seconds later near cross-shore distance x=65 m. The large variations in the location of the leading edge over time (near 91 minutes compared to just after 91.5 minutes) point out the difficulty of defining a swash zone for

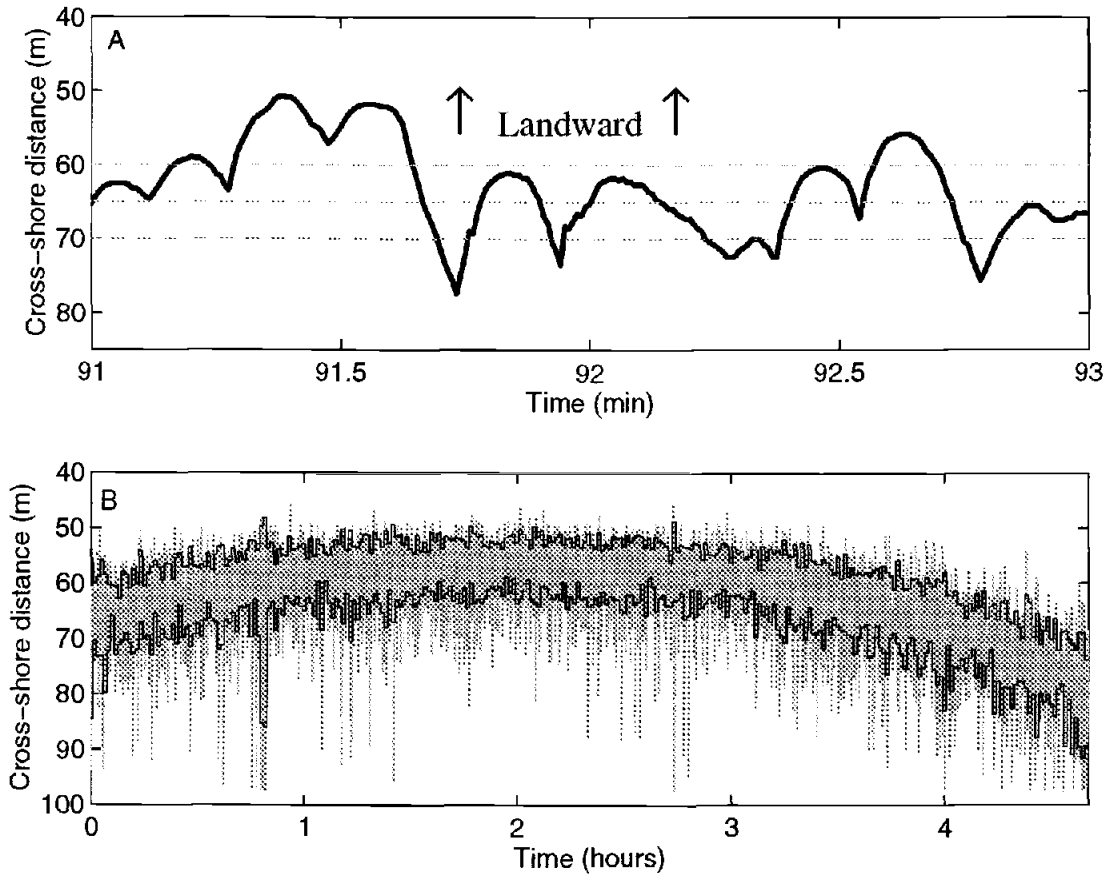

Figure 2.7. A) Two minute run-up time series with landward toward the top of the figure. The gray dashed lines correspond to the cross-shore location of the 3 instrument bars. B) Run-up time series for entire run (gray). Solid black lines correspond to mean ± 1 standard deviation as determined from 2 minute data blocks.

this Lagrangian swash signal. We would like to develop a working definition, however, so the location of the sensors with respect to the surf or swash zones can be determined. Figure 2.7B shows the run-up excursions for the entire data run (light gray) and the mean ± 1 standard deviation as determined from 2 minute data blocks (black). This may be a plausible estimate of the average swash zone width and location over time since it includes the mean leading edge location and a statistical spread about that mean. With this swash zone definition, Table 2.1 displays the percentage of time that the instruments were located within the swash zone. The calculations showed that the seaward sensors were located in the swash zone about 1/3 as often as were the landward sensors. The calculations were also done for the mean ± 2 standard deviations. In either case, the seaward sensors were in the swash zone much less than were the landward or middle sensors. In fact, using the 2 standard deviation width, shows that the landward and middle sensors were in the swash zone nearly the same percentage of the time (Table 2.1).

Power spectral density (PSD) calculations were performed on the video run-up time series data and band-averaged over 128 frequency bands to smooth the spectra. A broad spectral peak in the infragravity band was determined from the run-up PSD's for February 26, 27 and 28 (Figure 2.8). Since the swash zone was dominated by infragravity motions and the infragravity dominance increased over the 3 days (76 % to 94 %; Table 2.2), it might be expected that the foreshore would have eroded during this time. However, Holland and Holman (1997) noted that the beach was relatively stable (very few changes >10 cm) over the course of the experiment. As an example, Figure 2.9

Table 2.1. Percent of time the instruments were in the swash zone

Sensors	Swash zone width= mean± 1 std	Swash zone width= mean± 2 std
Landward	78	94
Middle	45	91
Seaward	27	57

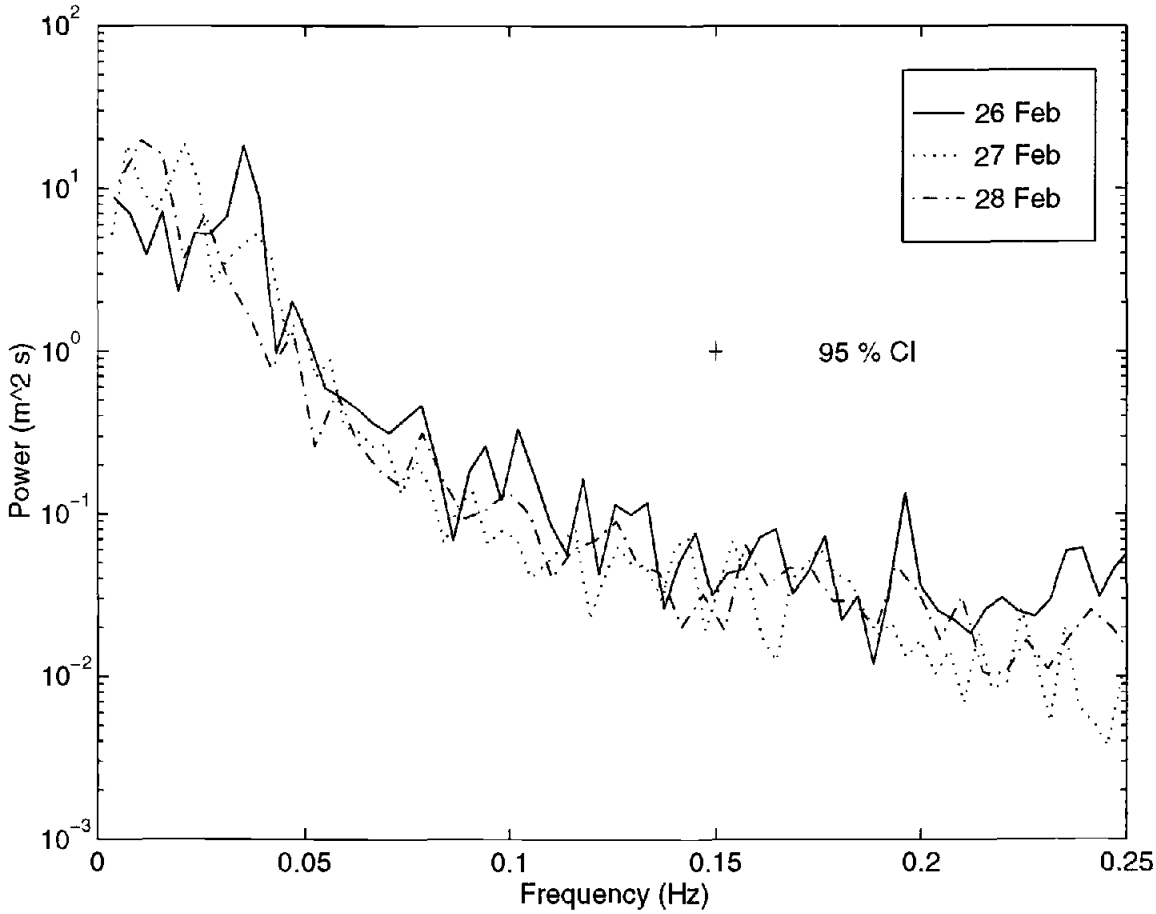

Figure 2.8. Band averaged power spectral density calculations on the continuous run-up times series from February 26, 27, and 28, 1994. Note the progressive decrease towards lower frequencies motions over the three days.

Table 2.2. Percent of run-up energy by frequency band

Frequency Band (Hz)	02/26/94	02/27/94	02/28/94
Incident (0.03 – 0.3)	24	20	6
Infragravity (0.003 – 0.03)	76	80	94

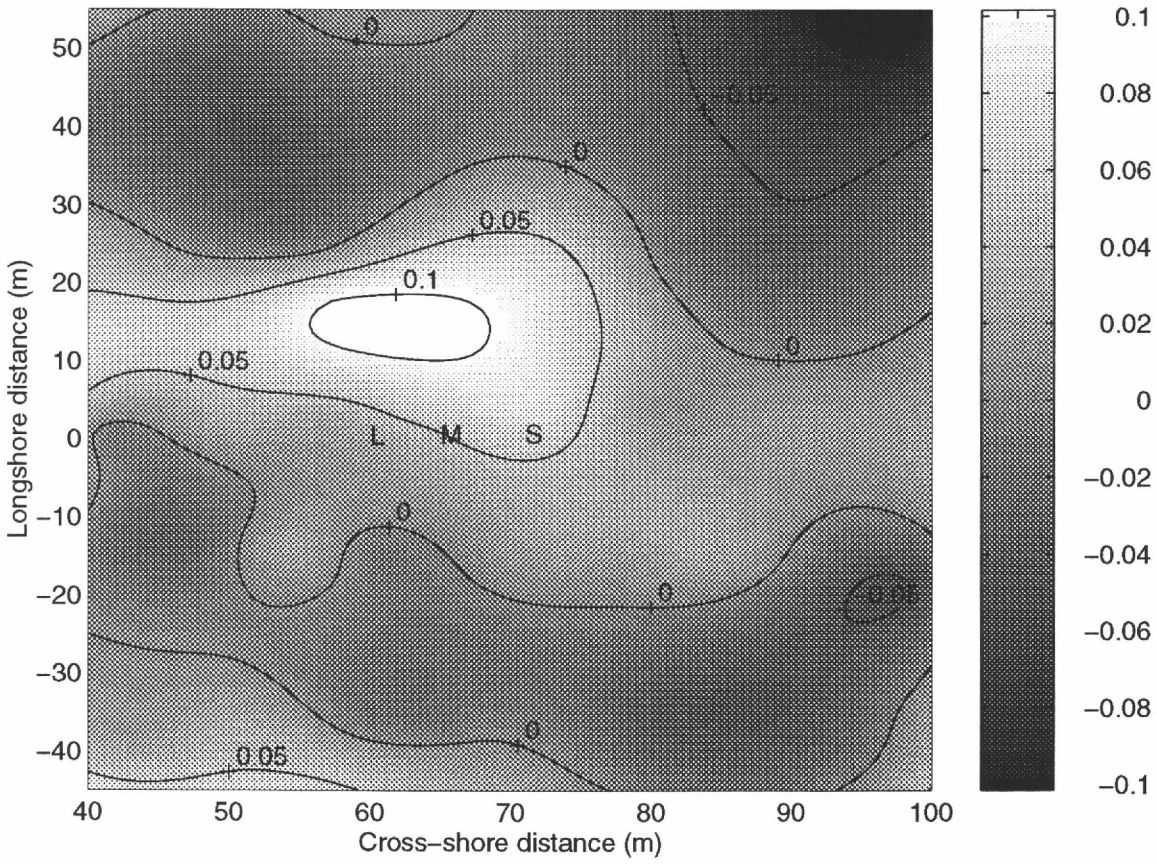

Figure 2.9. Difference map of foreshore surveys conducted on February 27, 1994. L, M, S correspond to the location of the Landward, Middle and Seaward sites respectively. The gray color scale corresponds to accretion (positive values, light shades) or erosion (negative values, dark shades) in meters.

shows the difference plot of foreshore surveys completed before and after the data run on February 27. The plot shows that near the FOBS instruments (Labeled L,M,S for landward, middle, and seaward respectively), the beach accreted approximately 5-10 cm in direct contrast to the expected erosion. This reinforces the need for a better understanding of sediment transport within the swash zone.

Bed-level determination.

An important aspect of FOBS data is the ability to determine the time-varying location of the bed and hence to accurately locate individual FOBS channels with respect to the bed. The average bed level over a 2 minute data block was estimated by locating the highest FOBS sensor with signal saturation. The two criteria for selection were: a) the output level was high, and b) the standard deviation was low. Specific calculations were:

1) A FOBS sensor was first considered saturated when the median SSC output for a 7 second block was greater than 15 % of the maximum output for that sensor. Over the two minute period, any sensors for which this occurred more than 80 % of the maximum number of times it occurred for any sensor was chosen as a bed level candidate over that data block.

2) The standard deviation of that data block was considered low when the standard deviation normalized by the mean (of SSC) over the data block was less than 0.35 times the maximum standard deviation normalized by the mean for any sensor over the 2 minute data block.

The sensor for which 1 and 2 occurred and the number of 7 second blocks a sensor was chosen as a bed level candidate over the 2 minute data block decreased monotonically for the 2 sensors above was considered the time varying bed level.

The bed level was estimated for the entire run and visually checked by eye to verify its validity. Furthermore, results from this bed level finding routine on a different data set compared favorably to the bed level determined by an alternate method (Foster, 1996).

The bed level fluctuations for each of the 3 cross-shore locations for February 27, 1994 are shown in Figure 2.10. At high tide, the landward bed level accreted approximately 3 cm and during the falling tide eroded approximately 4 cm. The bed at the middle location fluctuated by ± 3 cm over approximately one hour, possibly because it was farther seaward and may have experienced more suspension and transport. The most seaward sensors experienced greater erosion and accretion with the sediment level varying up to 10-11 cm over approximately one hour. At times the FOBS sensors were completely above the bed. The seaward sensors were, according to our swash zone definition, often in the surf zone (seaward of the swash zone) and may have been subject to shore break conditions. The bed level shows variability in both frequency and magnitude, with some small features being very transient while others persisted on the order of hours. The landward standard deviation of bed level was 1.09 cm while it was 2.87 cm for the seaward sensors. The larger standard deviation at the seaward sensors is reflective of the variability in bed level over the course of the run. In general, the sensors

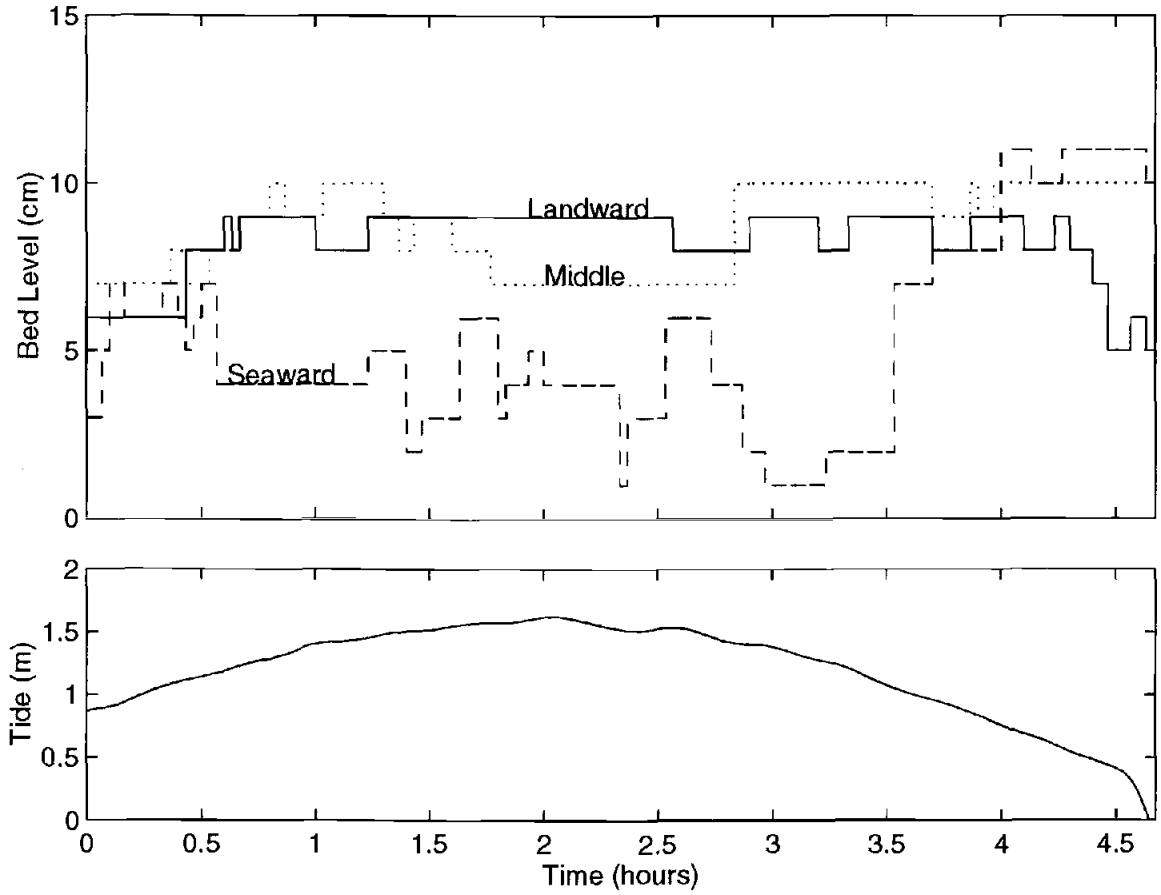

Figure 2.10. Bed level time series as determined from the finding routine for the 3 cross-shore locations for February 27, 1994 (upper panel). Tidal curve showing high tide at roughly the middle of the data run.

Table 2.3. Bed level statistics for 3 cross-shore locations

	Landward	Middle	Seaward
Range (cm)	4	3	10
Standard Deviation (cm)	1.09	1.30	2.87

show slight accretion at the beginning of the run (higher tide) and a larger range and variability towards the surf zone (Table 2.3).

Bed-level box-model

A simple bed level fluctuation box model can be used to test the accuracy of the bed level estimates and the degree to which sediment mass is conserved within the data set. The foreshore adjustment was modeled using a discretized version of the sediment mass balance equation

$$\frac{\partial h}{\partial t} = \frac{-1}{\rho\alpha}\frac{\partial \mathbf{Q}}{\partial x} \quad \Rightarrow \quad \Delta h = \frac{\mathbf{Q}_{landward} - \mathbf{Q}_{middle}}{5m}\frac{\Delta t}{\rho\alpha}, \tag{II.11}$$

where h is the bed level height, ρ is the sediment density, α is the solidity (=1-porosity) of the beach and the sediment flux, **Q** is given by

$$\mathbf{Q} = \int_0^{\zeta} u(z)c(z)dz, \tag{II.12}$$

where u is the velocity, c is the concentration at some height z and ζ is the water depth. The suspended load is defined as

$$\mathbf{C} = \int_0^{\zeta} c(z)dz. \tag{II.13}$$

Because the FOBS sensors often span a limited range of the water column compared to η, **Q** and **C** were in general calculated up to ζ, defined as the height of the sensors or the water depth, whichever was less. In analyzing sediment transport, the estimated sediment flux was evaluated in one of two ways: using II.12 above (method 1). Alternatively, we determined the suspension profile to the surface assuming a linear profile to zero concentration at the surface if η was above the highest sensor (method 2). Because there were only 2 current meters, a stepped velocity profile (defined as the lower velocity up to mid-point between the two current meters and the upper velocity for the water column above) was used to estimate the sediment flux.

Figure 2.11 shows the bed levels determined directly from the FOBS data (solid line =landward location, dashed line=middle location) and the simple model results (bold curves). The dotted bold curve is the model calculated using method 1 above, while the solid bold curve uses method 2 from above. Clearly, the simple model works quite well for the first 60 minutes of the run regardless of whether or not the suspension profile is extended to the water surface (method 2). The gap in the curves just after 60 minutes occurred because the bed level accreted and interfered with the current meter at the middle location, rendering a false flux calculation. As the bed level eroded a few centimeters (approximately 120 minutes) the models diverged. Extending the suspension profile to the water surface (method 2) caused the model to over-predict the bed level by 10 cm. However, using method 1 above and not accounting for any sediment above the sensors caused the model to under predict the bed level by roughly 4 cm. While we are unable to quantify sediment fluxes above the sensors, we are encouraged that the

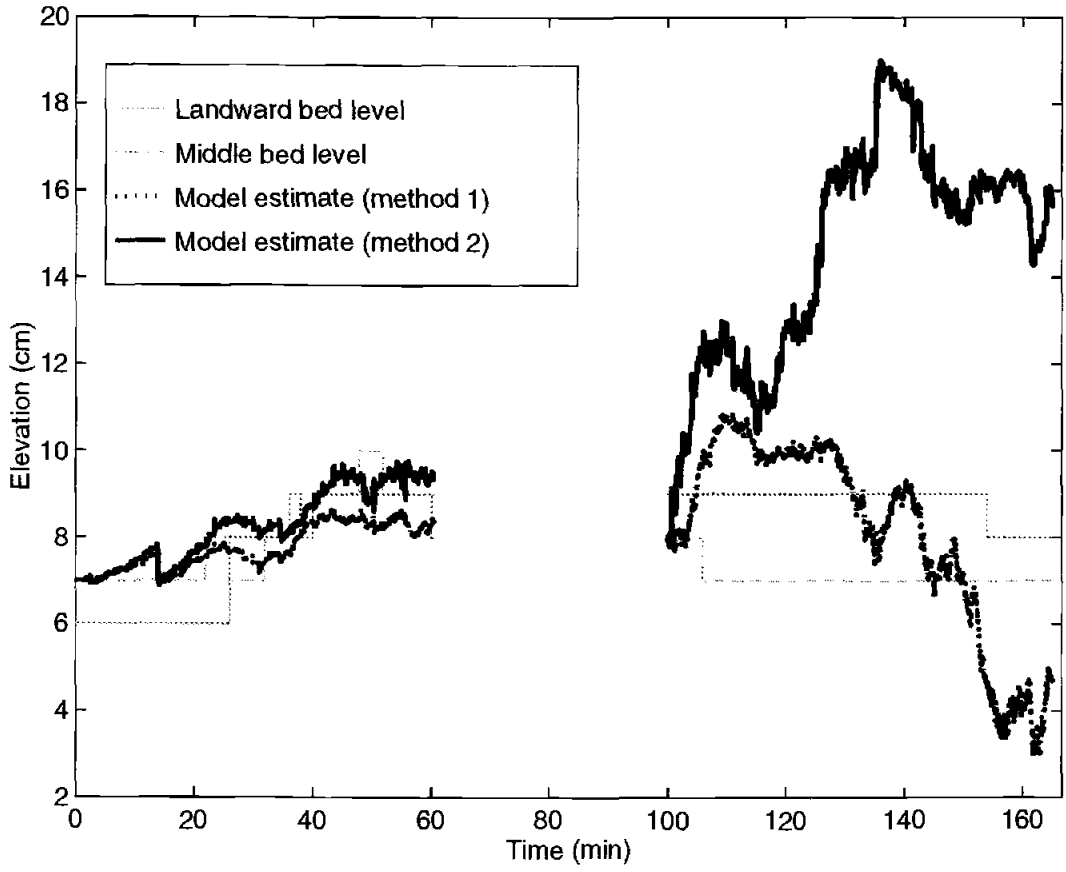

Figure 2.11. Bed levels for the landward (gray solid line), middle (gray dashed line) and corresponding model calculations. The bold dotted model curve did not estimate sediment flux above the sensors. The bold solid model curve used a linear interpolation to the surface to estimate the sediment flux above the sensors. Gaps in bed level are a result of accretion interfering with current meters.

conservative (method 1) and high (method 2) estimates bracket the observed beach change. Some errors are most likely introduced through the use of a stepped velocity profile, FOBS signal saturation which may underestimate c, and by the omission of bedload. In addition, the model may perform better during the beginning of the data run when the tide was not quite as high because less of the water column was unsampled (above the sensors).

Spatial characteristics in sediment suspension

Even though the swash zone is a Lagrangian region within the nearshore, sediment suspension will be analyzed by monitoring swash motions passed fixed sensors. Cross-shore variations in the vertical structure of sediment suspension were analyzed once the time varying bed level elevations had been extracted from the record. Figure 2.12 shows an example 54 second time series color plot of suspended sediment concentrations for all 3 instrument locations. Contouring terminates at the highest FOBS sensor. The evolution of swash events can be seen from surf zone to swash zone as the water depth (dashed lines) and sediment concentrations increase first in the lower panel (most seaward, Figure 2.12C) and progressively at later times to the middle (Figure 2.12B) and upper (most shoreward, Figure 2.12A) panels. After flow reversal, the backwash progresses offshore to a shallow water depth (< 10 cm) at the lower panel, implying that at this time the seaward instruments may be considered in or very close to the swash zone. One can follow the next uprush and ensuing backwash from lower to upper panels. It is interesting to note that what appears as two events at the landward

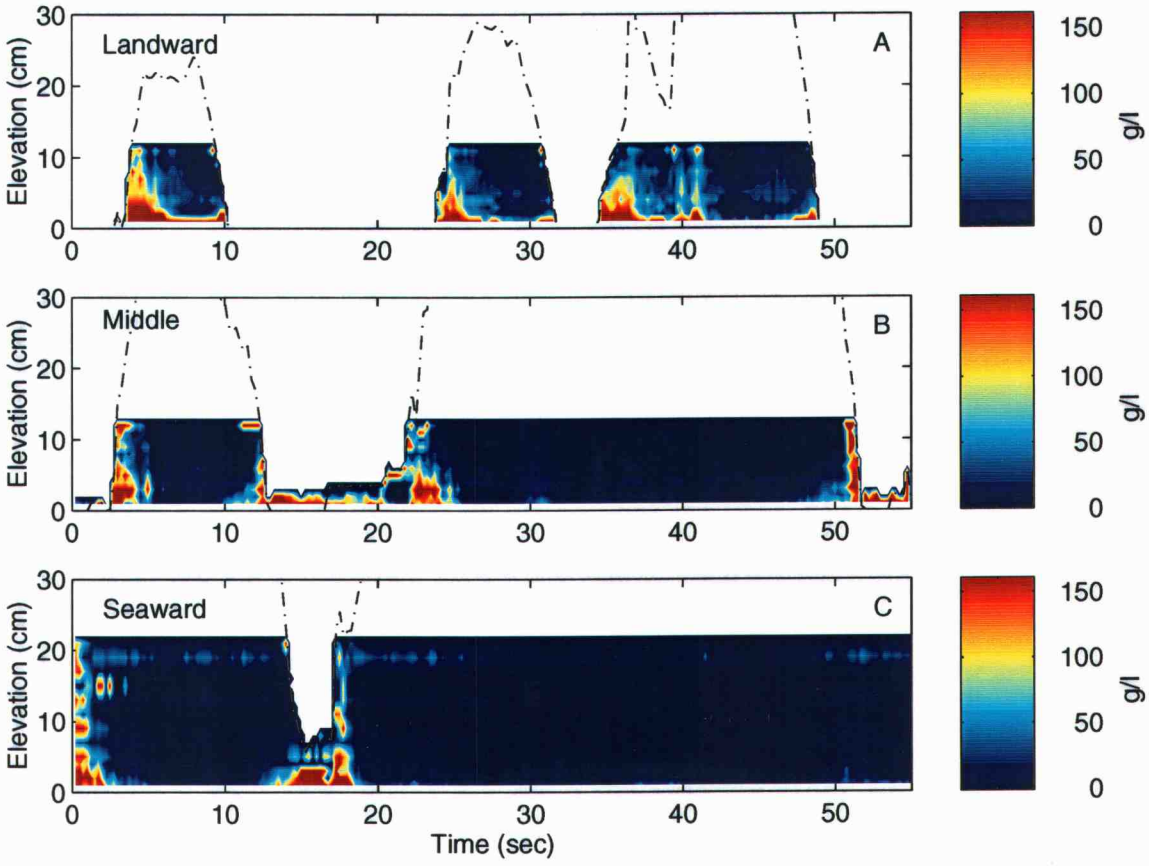

Figure 2.12. Cross-shore variations in suspended sediment concentration. Displays a progression of swash events and associated sediment suspension from the seaward (C) to middle (B) to landward (A) sensors in the swash zone. The dashed line corresponds to the water depth. The color map terminates at the highest FOBS sensor.

sensors (near 35 seconds) is seen as only 1 event at the middle and seaward sensors. Furthermore, the seaward sensors appear to be in the surf zone and record little suspended sediment in the water column except below the shoreward progressing bore. The backwash did thin considerably at the middle location (approx. 51 seconds) and hence the middle sensors were probably affected by swash processes and could have been considered in the swash zone. These spatial characteristics imply that the swash zone is a continually shifting region of the nearshore. Although the boundary between the surf zone and swash zone is not well defined, it appears that the transition may occur in a short (~5 m) cross-shore distance or roughly 50 cm vertically on a steep beach such as this.

The intense SSC signal observed in the toe of the uprush may suggest that bubbles were responsible for the signal. However, Sternberg *et al.*, (1984) showed in a recirculating calibration tank that bubbles did not influence the signal recorded by OBS instruments. FOBS sensors have also been tested in recirculating tanks with similar negative results. Furthermore, if bubbles were responsible for the observed SSC signal, then we might expect an inverse gradient in SSC since bubbles rise as they are advected with the uprush passed the sensors. Sustained or pronounced inverse gradients such as this were not observed in the data and hence the recorded SSC would be indicative of the actual suspended sediment concentration.

Examples of backwash thinning and possible boundary layer thickening can be seen as the water depth pinches to zero near 10 and 50 seconds (Figure 2.12A). Shortly before 10 seconds, the suspended sediment concentration increases at the landward

sensors (Figure 2.12A), and only a few seconds later (Figure 2.12B) as the backwash accelerates downslope and thins, the suspended sediment concentration, although near the same magnitude, is carried higher into the water column. The sediment suspension is high at the seaward sensors also (Figure 2.12C), but is not carried higher into the water column because the water depth does not continue thinning as the backwash approaches mean sea level. This type of suspension is even more evident shortly before 50 seconds, as suspended sediment concentration increases at the landward sensors (Figure 2.12A), but is confined near the bed. As the backwash continues downslope (Figure 2.12B), the high (~ 150 g l^{-1}) suspended sediment concentrations extend vertically through the water column possibly due to the increase in backwash duration. No substantial increase in suspended sediment concentrations is observed at the seaward sensors (Figure 2.12C) at this or a short time following, again implying the short cross-shore transition from swash to surf zone conditions. Lastly, the long duration event observed at the middle sensors (Figure 2.12B), may be indicative of high suspension events occurring on longer (> than incident band periods), time scales within the swash zone. Hence, we may expect that the manifestation of infragravity energy in the swash zone is indicated by longer duration motions.

It appears from the data that advection may be a very important consideration in swash zone sediment transport. In figure 2.12C, the intense SSC signal is observed in the leading edge of the swash and a very similar signal can be seen in the leading edge as it traveled passed the middle and landward sensors only a short time later. Suspended load calculations of the uprush maximum for these few seconds of the run (0-5 seconds;

Figure 2.12) showed a progressive decrease from 2.26 g cm $^{-2}$ to 1.48 g cm^{-2} to 1.29 g cm^{-2} from the seaward to the landward sensors. If sediment settling and the fact that there was more vertical coverage (due to an increase in the FOBS probe head spacing) at the seaward sensors are considered, then it appears that the suspended load at the landward sensors for this uprush may have been advected from the seaward sensor location and not necessarily re-suspended from the bed in the direct vicinity of the landward sensors.

The sediment suspension associated with this cross-shore time series shows most of the high suspension occurring closer to land, as can be seen at the landward sensors. Large cross-shore gradients in SSC can be seen to occur over a length scale as short as 5 – 10 m (Figure 2.12). Approximately 2-4 seconds after the leading edge traveled beyond the seaward sensors, the suspended sediment concentration declined drastically while during that time the suspended sediment concentration at the landward and middle sensors was extremely high with values near 100 g l^{-1} up to 8 cm in the water column. These strong cross-shore gradients can be noted throughout the run and also appear in the mean suspended sediment profiles that were calculated when the sensors were immersed (Figure 2.13). The landward and middle sensors have similar mean suspended sediment profiles with near bed values greater than 50 g l^{-1}. The seaward sensors have SSC values less than the other two locations and are more typical of surf zone profiles (little sediment in suspension except close to the bed) with the SSC decreasing rapidly away from the bed. The suspended load calculated to the highest sensor increased in the landward direction with the values ranging from roughly 0.28 to 0.47 g cm^{-2}. The slight

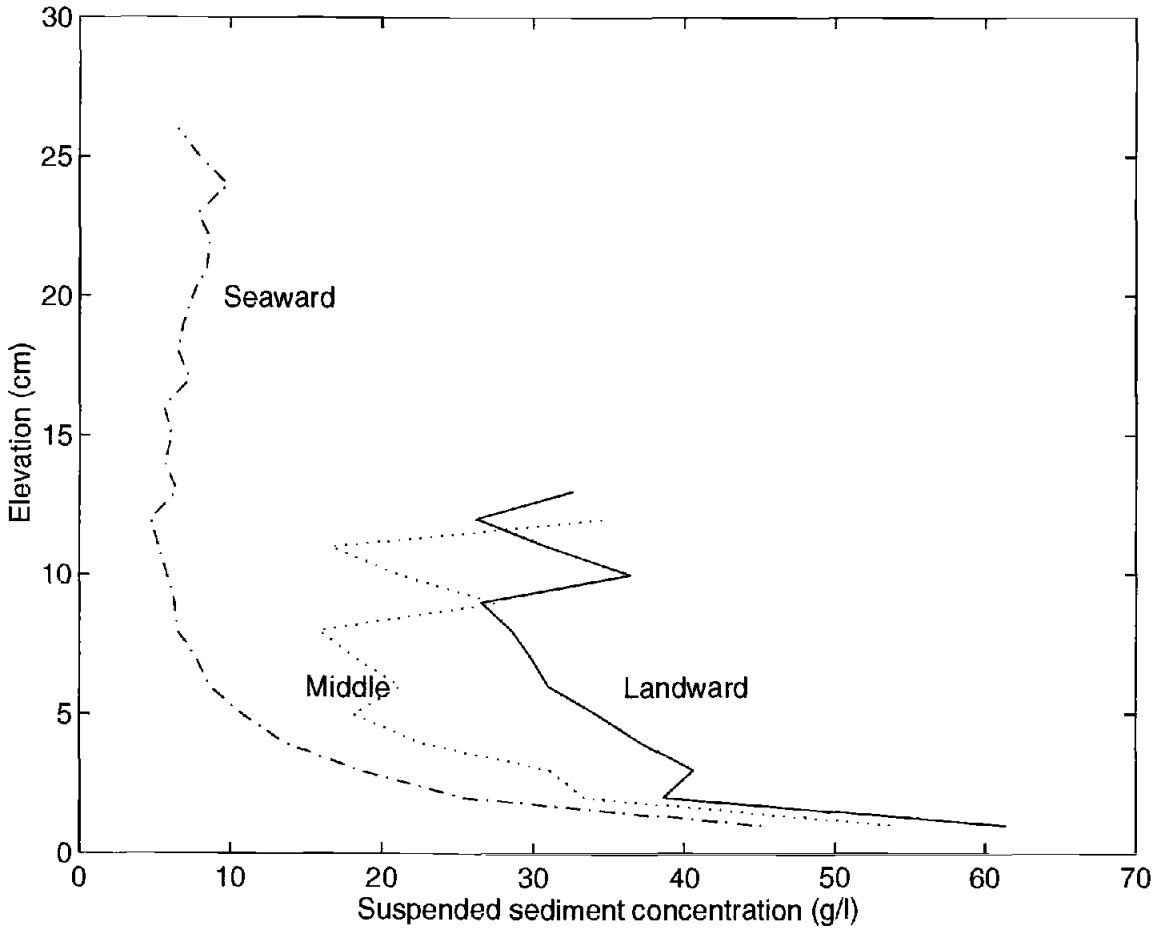

Figure 2.13. Mean suspension profiles when sensors submerged. Inverse gradients at the landward and middle locations are probably a result of surface foam advection. More vertical coverage was obtained at the seaward sensors due to increased FOBS sensor spacing.

inversions seen in the upper few centimeters at the landward and middle sensors could be due to foam floating on the water's surface. If the water depth was slightly over estimated with respect to the FOBS data, then the profiles may include sensors above the actual water line. Since the sensors were designed to measure suspended sediment and not surface foam, these high values of backscatterance could be recorded as SSC. Note that this is a different issue from false signals due to bubbles, previously shown to be insignificant.

Temporal characteristics in sediment suspension

Ensemble averaging

The velocity time series was used to determine swash duration by analyzing zero crossings in the velocity record. A swash event is defined as the water motion within the landward and seaward phases of a swash cycle that originates and terminates at a specific cross-shore sensor. It is important to note that a swash event is not the entire swash cycle nor is the duration based on wave period. An example of a swash event can be seen in Figure 2.12A where the swash motion starts at roughly 4 seconds and ends near 10 seconds at the landward sensors. Although the entire swash cycle is probably on the order of 18 seconds (as evidenced by the motion past the seaward sensors), the swash event in question involves the motion about the landward sensors only. Swash events of 6, 9, and 12 seconds duration were analyzed for the landward and middle sensors. To obtain ensemble averages, a certain duration event was allowed to vary for 0.25 seconds

before to 0.5 seconds after the nominal chosen length. For instance, a 6 second event could be in the range between 5.75 and 6.5 seconds long. In order to examine the mean suspended sediment concentrations within a swash event, a re-grid technique based on interpolation was used to normalize the swash lengths for 6, 9 , and 12 seconds. Furthermore, swash events were reviewed by eye to choose those that had roughly the same velocity characteristics and had initial and final water depths of no more than 10 cm. Although this may contradict some definitions of the swash zone (seaward edge of the swash zone is located where bore collapse occurs implying the initial water depth should be at or very near zero), an initial or final depth of 10 cm implies only approximately 1 m cross-shore distance to dry foreshore based on the beach slope. So, if the swash zone was 10 m (20 m) wide this would equate to roughly 10 % (5 %) of the width.

Temporal variations in sediment suspension

Contour plots of the 6, 9, and 12 second ensemble average swash events (Figure 2.14A, Figure 2.15A, and Figure 2.16A, respectively) show the suspended sediment concentrations as they evolve through time. Again, the contouring terminates at the highest FOBS sensor. Time zero is the first indication of the landward flow as the bore passed the sensors. After flow reversal, a decrease in water depth occurred as the swash accelerated downslope and thinned. In all cases, the toe of the uprush is characterized by high SSC (exceeding 100 g l^{-1}). In the case of 6 seconds (Figure 2.14A), the SSC was 80-120g l^{-1} in the elevation range of 1-3 cm above the bed and was fairly uniform (40-60

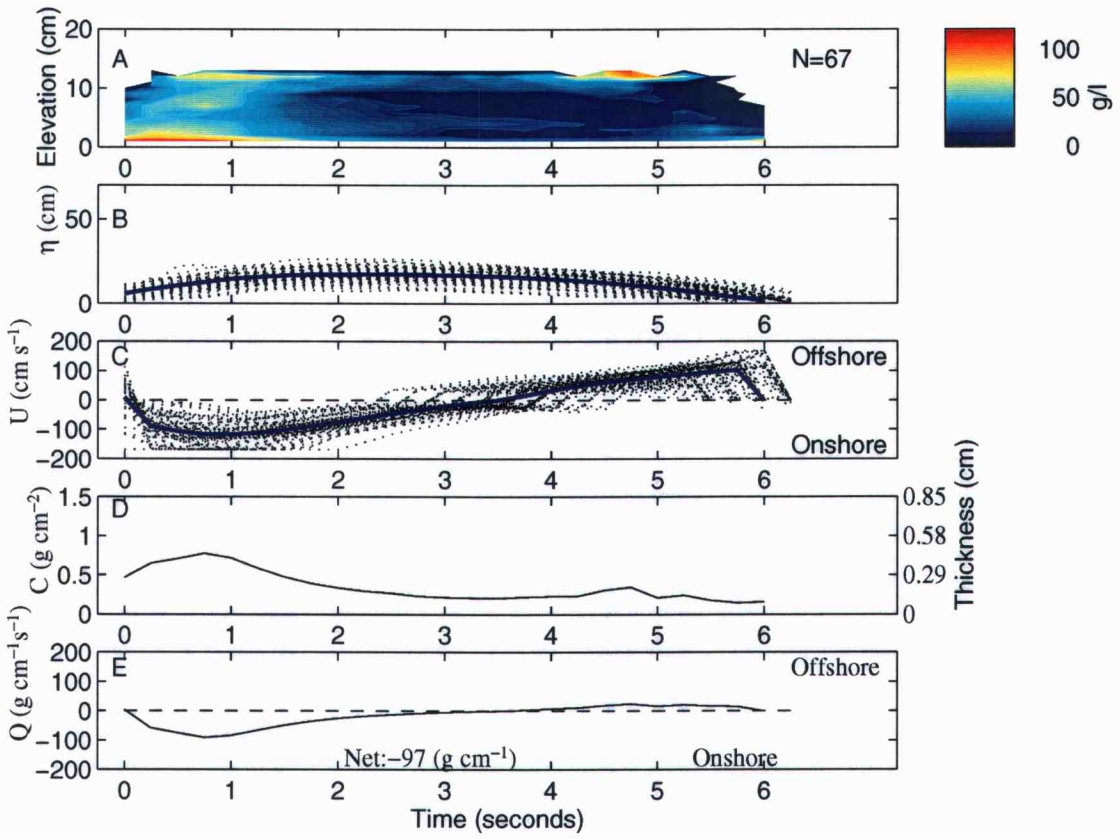

Figure 2.14. A) Six second ensemble average of suspended sediment concentrations for landward and middle sensors. B) Sea surface profiles of the chosen events (dotted curves) and the ensemble average sea surface profile (blue curve). C) Velocity profiles of the chosen events (dotted curves) and the ensemble average profile (blue curve). Negative velocities are onshore flow, positive are offshore. D) Suspended load over 1 cm^2 of bed obtained by vertically integrating the suspended sediment concentration over the range of the sensors. Equivalent "thickness" (right y axis) is the thickness of bed material that would result if the calculated suspended load was allowed to settle. E) flux estimates obtained from the product of the velocity (C) and suspended load (D) assuming a uniform velocity profile.

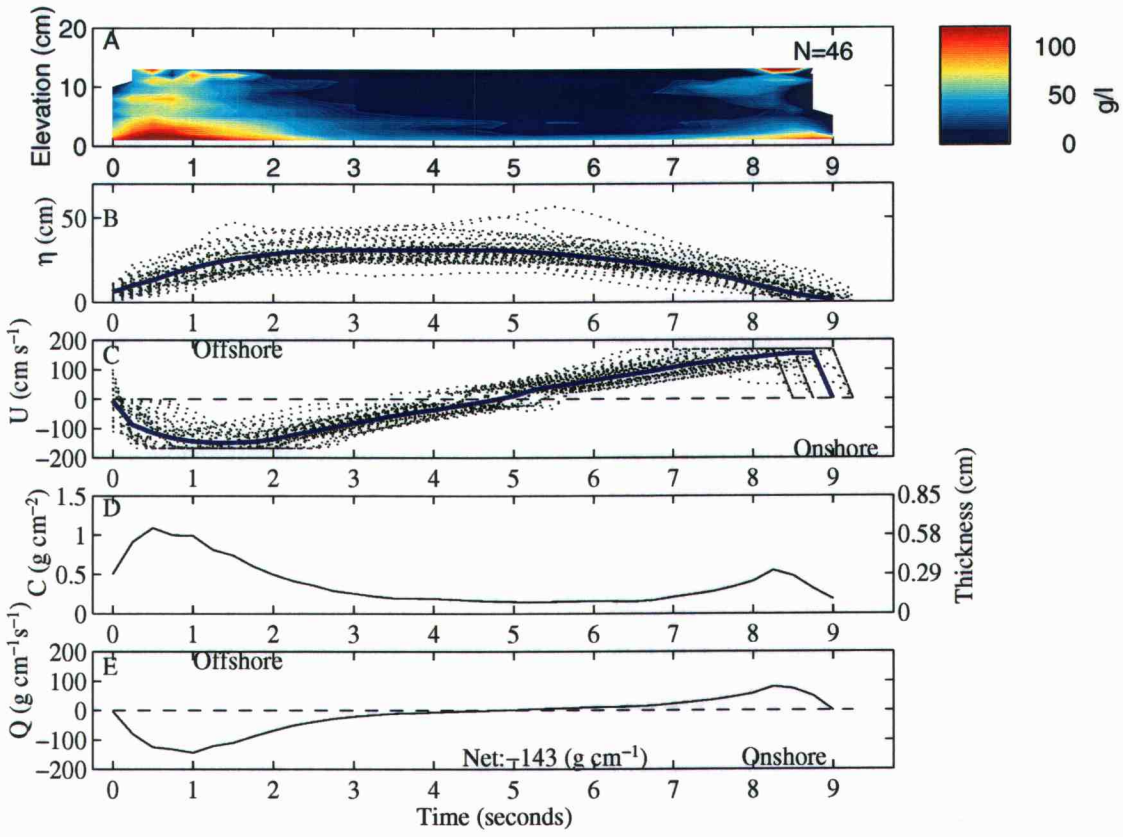

Figure 2.15. Nine second ensemble average. Panels as per Figure 2.14.

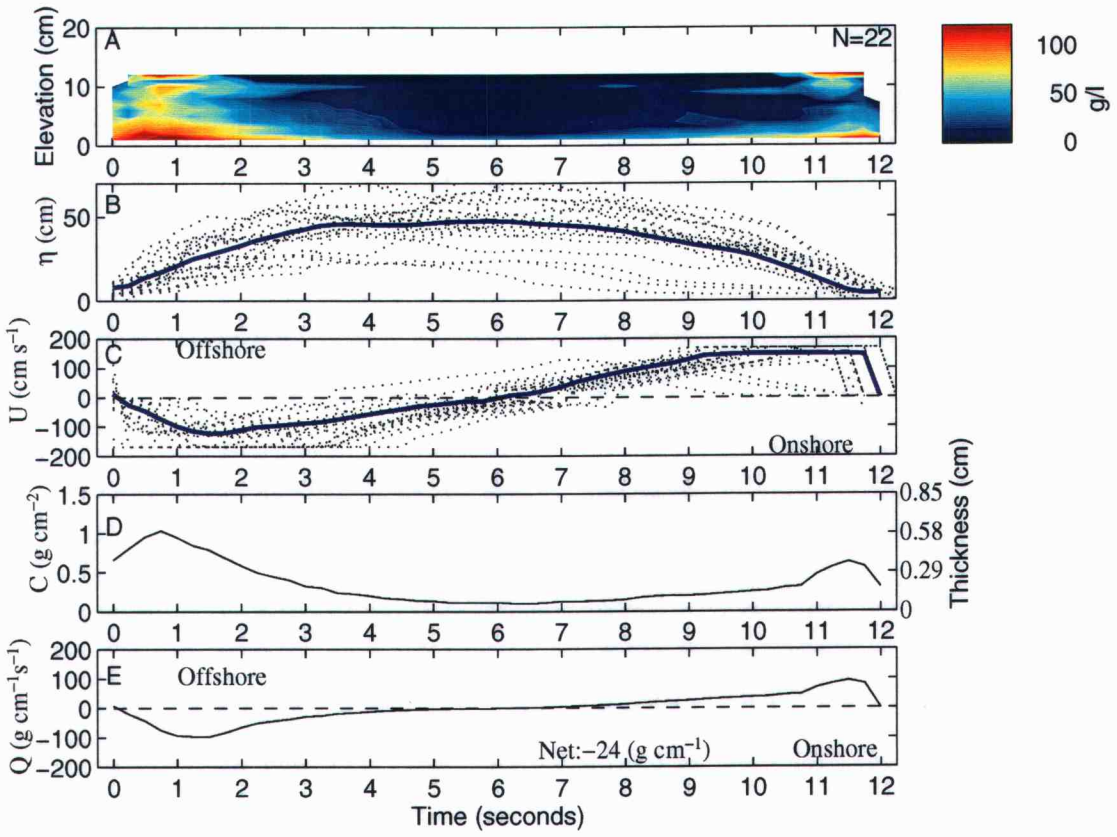

Figure 2.16. Twelve second ensemble average Panels as per Figure 2.14

g l^{-1}) over the rest of the range of the sensors . The 9 and 12 second events had similar characteristics with high (80–120 g l^{-1}) SSC values in the 1-4 cm above the bed and were fairly uniform (60-70 g l^{-1} and 70-80 g l^{-1}, respectively) over the rest of the range of the sensors. The suspended sediment concentrations then decreased rapidly as the swash front passed the sensors. The SSC was less than 20 g l^{-1} a few seconds after inundation and confined to within 1-3 cm of the bed in all cases. The standard deviation was approximately 30-40 g l^{-1} in the lowest few centimeters of uprush in all cases and decreased to about 15 g l^{-1} higher in the water column. The backwash suspension was different from the uprush suspension in that there was less sediment suspension up into the water column and the high SSC's (up to 120 g l^{-1}) were confined to just above the bed where strong vertical SSC gradients existed. This latter type of suspension is not seen in the 6 second ensemble average perhaps because the backwash did not have time to fully develop (Figure 2.14A). Backwash suspension for the 9 and 12 second cases increased slowly as the backwash accelerated downslope and continued to develop, possibly becoming turbulent. Coincident with this downslope acceleration was an increase in SSC as the sediment was carried slightly higher into the water column, yet the suspended sediment still remained close to the bed when compared to the uprush suspension (Figures 2.15A, 2.16A). An increase in the amount of backwash suspension can be seen from 6-9-12 seconds (Figures 2.14A, 2.15A and 2.16A), implying that swash duration may play a role in backwash sediment suspension. As previously stated, the high SSC's seen at roughly 11 cm could be due to surface foam advecting passed the uppermost FOBS sensors.

Figure 2.17 shows the mean vertical profiles from the first second (uprush) and last second (backwash) of the ensemble events. In all three cases, the uprush SSC is up to a factor of 2 larger than the backwash SSC near the bed and up to 7 times larger than the backwash SSC at 5 cm above the bed. These profiles quantitatively display the vertical structure between uprush and backwash suspension as well as the dominance of uprush SSC compared to backwash SSC. The extreme increase in SSC in Figure 2.17B,C at z=13 and z=12 cm, respectively for the backwash profile is most likely due to surface foam advection.

Figures (2.14B, 2.15B and 2.16B) display the water depths for the events that were chosen. The blue curve is the ensemble average water depth for each duration. It can be seen that the maximum water depths at the sensors increase as duration increases.

Figures (2.14C, 2.15C, and 2.16C) show the velocity structure for each chosen event as well as the ensemble average normalized velocity structure. The hysteresis, abrupt jumps across zero in the velocity time series (Figure 2.14C; between 2.5 and 4.5 seconds), is due to the inertia (finite response time) of the ducted impeller current meters. Maximum measured cross-shore velocities were found to exceed 167 cm s^{-1} and the clipping noted at this value was a result of the maximum sensor output. Although the velocity profiles look similar, flow reversal (velocity zero crossing) occurred within a 2 second window. This window could be important for backwash suspension as a shorter backwash may have less time to develop and suspend sediment. In all cases, the average

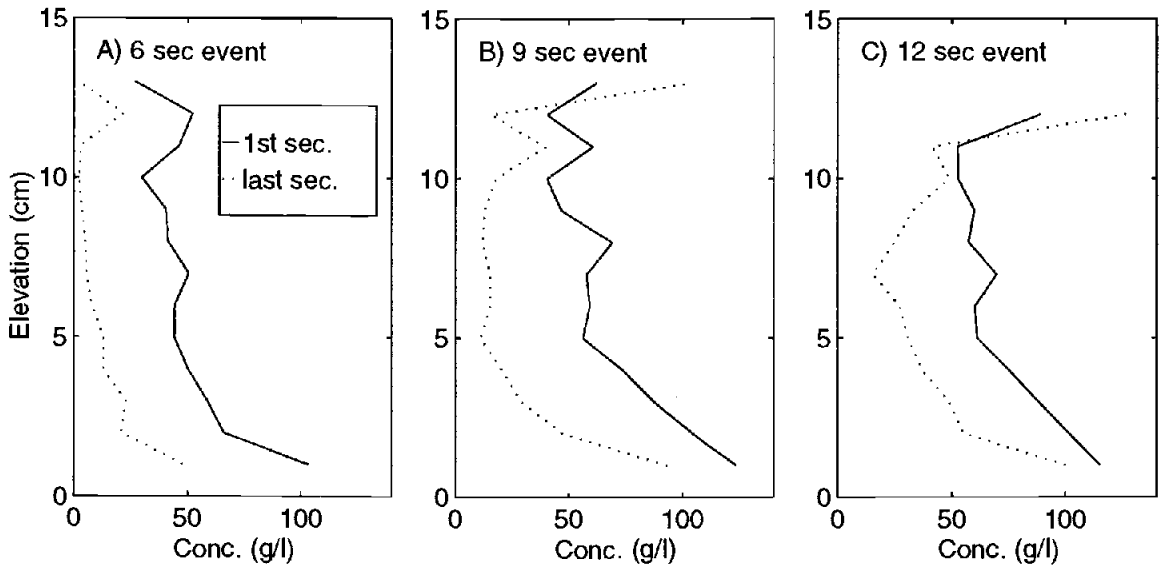

Figure 2.17. Mean uprush (during first second from ensemble average) and backwash (during last second from ensemble average) profiles over the range of the sensors. A) Six second events. B) Nine second events. C) Twelve second events. The inverse gradients in B,C could be due to surface foam advection.

flow reversal occurs at or after the mid-point of the swash event. It is not surprising that the backwash in the 6 second event did not suspend much sediment as the ensemble average backwash was only 2.5 seconds in duration (Figure 2.14C). Ensemble average backwash duration was approximately 1.5 seconds longer for the 12 second events (Figure 2.16C) than for the 9 second events (Figure 2.15C) and may explain the greater amount of suspension in the 12 second events versus 9 second events.

The suspended load, C, is shown for the 6,9,12 second events in Figures 2.14D, 2.15D and 2.16D, respectively. Because the suspended sediment concentration above the FOBS sensors were not estimated, the reported C values are conservative. The suspended loads were very high in the uprush (approximately 1 g cm^{-2}), corresponding to high SSC, but reached their maximum values shortly after inundation due to an increase in water depth. The uprush suspended loads were similar in the 9 and 12 second events and slightly less for the 6 second event. Following the first 1-2 seconds of intense suspension, C decreased rapidly and remained roughly constant (approximately 0.25 g cm^{-2}) through flow reversal. C increased again as the backwash began and reached values near 0.5-0.75 g cm^{-2} (Figures 2.15D and 2.16D). The suspended load did not increase in the backwash of the 6 second case as there was little backwash suspension. In all cases, the suspended load within the first 1.5 seconds of the uprush (the motion associated with leading edge) accounted for >60 % of the total uprush load.

The equivalent "thickness", defined as the amount of sediment that would need to be eroded to obtain the observed suspended loads ($\Delta h = C/[\{1-\alpha\}\rho_s]$), was determined

assuming ρ_s=2.65 g cm^{-3} and α= 65 %. In all cases, about 0.5 cm would need to be eroded to maintain the observed uprush suspended loads while about 0.3 cm would need to be eroded to maintain the backwash suspended loads for the 9 and 12 second events. With little suspension in the backwash of the 6 second event, only about 0.05 cm would need to be eroded. These simple calculations imply that the top 1 cm of sediment on the foreshore must be very active.

The product of the ensemble average velocity (<u>) and ensemble average suspended load (<C>) yielded the time-dependent cross-shore sediment flux (Figures 2.14E, 2.15E and 2.16E). The velocity is from the lowermost current meter and is assumed uniform over the water column and should yield a conservative estimate since the lowermost current meter is most likely within the boundary layer. The largest of the sediment fluxes occurred in the uprush when the velocity and suspended loads were at a maximum. Peak flux values were over 140 g $cm^{-1}s^{-1}$ in the 9 second event and about 100 g $cm^{-1}s^{-1}$ for the 6 and 12 second events. Net transport was partially a function of swash duration as all ensemble average events had high sediment transport in the uprush, but differed considerably in the backwash with offshore transport increasing with flow duration. Net transport was always onshore for the 3 durations chosen and the amount of net shoreward transport decreased with increasing swash duration from 9 to 12 second events. The net transport being onshore for these events is consistent with the beach surveys conducted at Glenedden (Figure 2.9). Specifically, the foreshore above the landward sensors accreted approximately 5 cm which agrees fairly well with the conservative flux calculations for the entire run at that cross-shore location.

Testing the Bagnold-type equation

Instantaneous immersed weight transport rates, $i=uCgs$ where $s=(\rho_s-\rho)/\rho_s$ and ρ_s is the sediment density, were plotted against II.5 assuming $U_s=u$ to test the Bagnold-type equation (Figure 2.18). The data for the both instantaneous onshore (Figure 2.18A) and offshore (Figure 2.18B) immersed weight transport rates are scattered with the largest r^2 values of 0.53 and 0.51 respectively. Both r^2 values were significant at the 99 % level (Appendix A).

Figure 2.19A and Figure 2.19B show the total immersed weight uprush and backwash transport $I=\int uCgs\partial t=\Sigma(uCgs\delta t)$, where δt is the data recording interval (1/4 sec.), for N=740 swash events plotted against II.5 times the flow duration, Δt. The mean velocity, $\bar{u}$, was determined from the mean of the observed instantaneous uprush and backwash velocities. Linear regression yielded r^2 values of 0.58 and 0.38 for the uprush and backwash respectively. In both cases, the r^2 values were significant at the 99 % level. The r^2 values were similar to the corresponding values for instantaneous transport rates (Figure 2.19A,B) with none of the r^2 values yielding very good correlations. Hence, these simple calculations have demonstrated a deficiency in the ability to predict sediment transport in the swash zone via a Bagnold-type formulation

Because the Bagnold-type sediment transport relations are proportional to a power of the velocity, the analysis is sometimes simplified by using u^n (n=2,3,4) as a simple surrogate for the Bagnold-type relation. So, in order to compare the transport

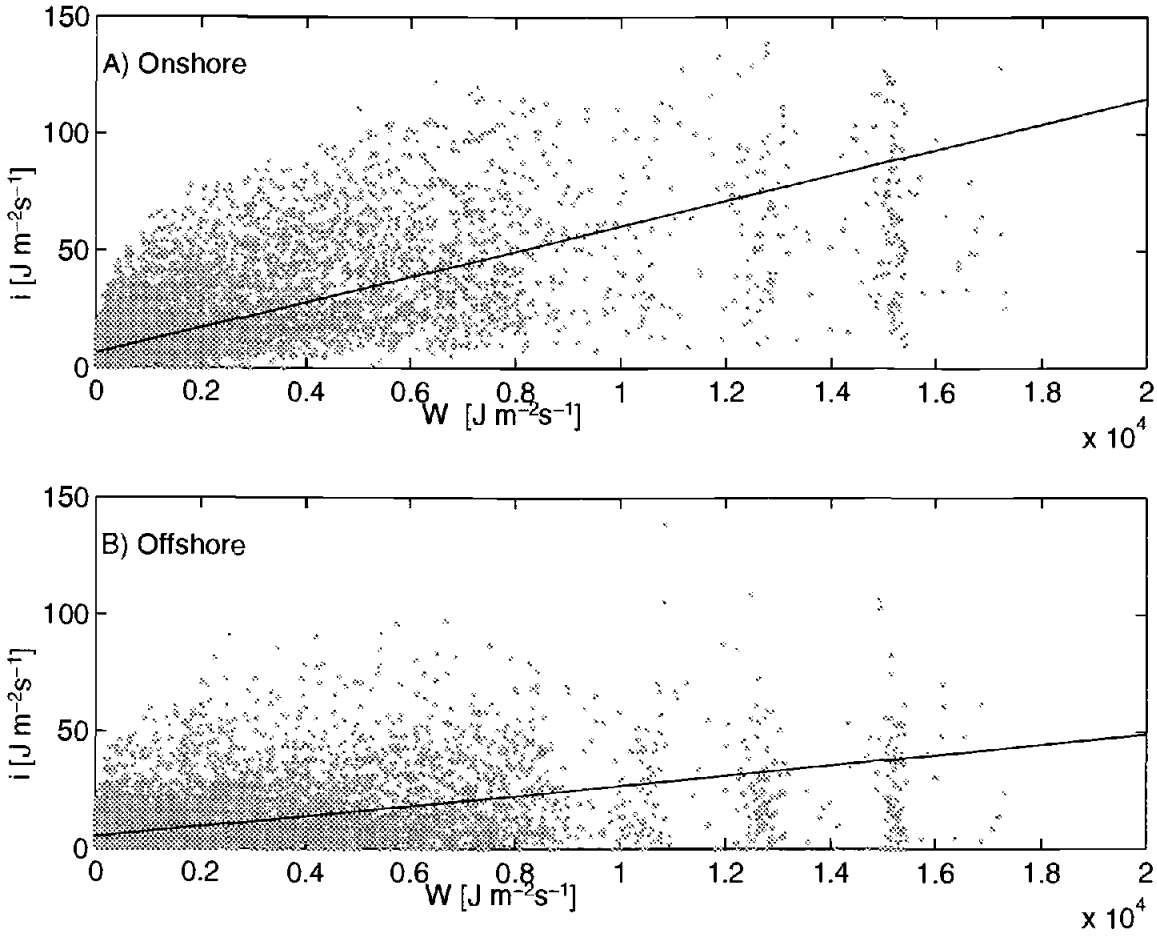

Figure 2.18. Linear regression of instantaneous immersed weight transport, i, onto W, the Bagnold-type transport equation. A) Onshore flow, N=10880, r^2=0.53 at the 99 % significance level. B) Offshore flow, N=11337, r^2=0.51 significance at the 99 % level.

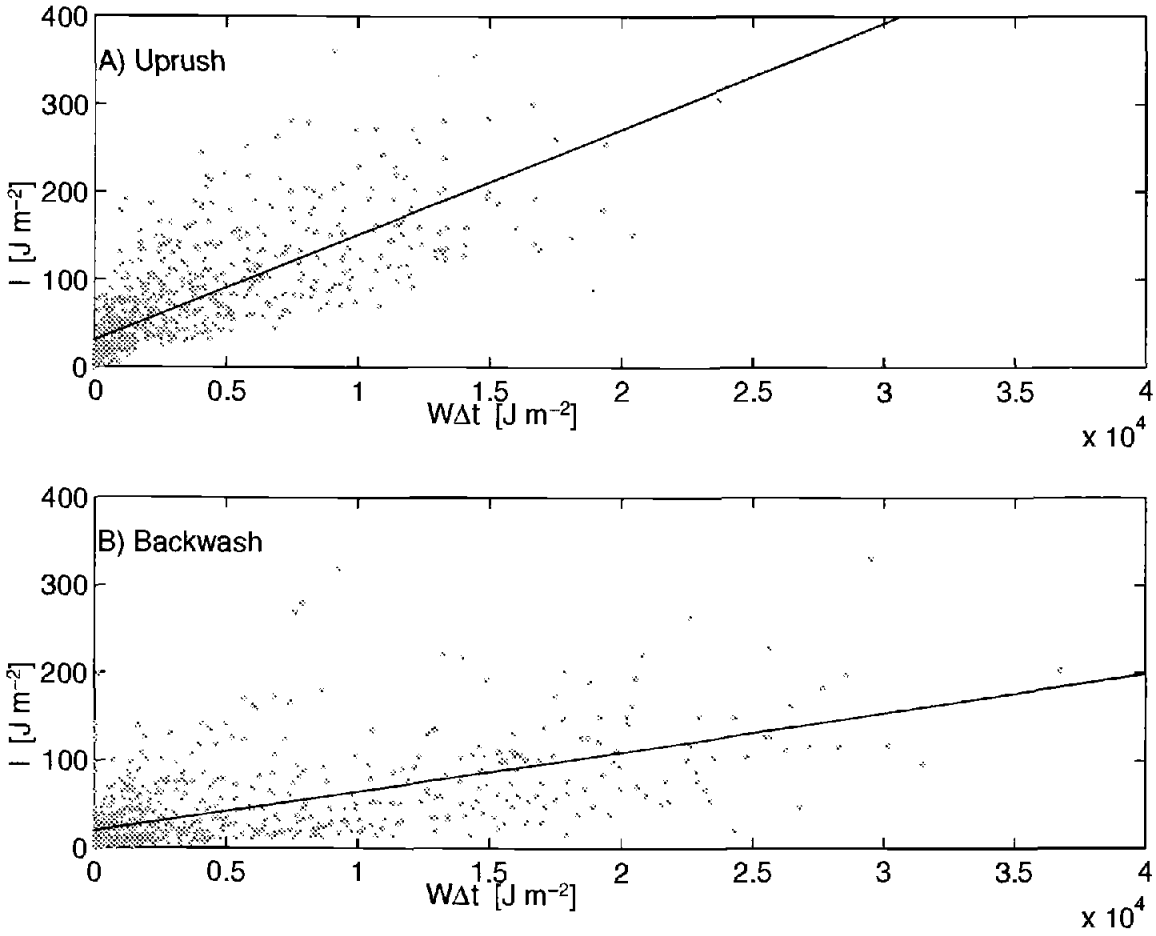

Figure 2.19. Linear regression of total immersed weight transport, I, onto WΔt. A) Uprush transport, N=740 swash events, r^2=0.58 significant at the 99 % level. B) Backwash transport, N=740 swash events, r^2=0.38 significant at the 99 % level.

observations from this study to those of other experiments, i was regressed onto u^n (n=2,3,4) and I, the total uprush and backwash transports, was regressed onto $\overline{u}^n\Delta t$, (Table II.4). These r^2 values show that the sediment transport in the uprush and backwash is better predicted by a u^2 relationship rather than a u^3 or u^4 relationship. Furthermore, the correlations increased for total transport in the backwash but decreased for total transport in the uprush when compared to their instantaneous counterparts. The slope coefficients were 2.92 and 2.26 for the total uprush transports for n=2 and n=3 respectively which are comparably to the values found in other studies (Hughes *et al.*, 1997). While these reported r^2 value show some dependence on u^2, it does not appear that the more appropriate Bagnold-type surrogate (n=3,4) or the entire Bagnold-type equation are adequate on their own in predicting the observed sediment transport. Results will be presented in the next section to justify this claim.

Turbulent dissipation and sediment transport

In order to assess the importance of bore generated turbulence to swash zone sediment transport, all swash events from the record that had the following criteria were analyzed: 1) h_2-h_1>1 cm, 2) $u_1 \neq 0$, 3) $h_1>0$ and 4) $Fr_1>1$ and $Fr_2<1$. These criteria were chosen in order to increase our confidence that the dissipation calculated was actually across the bore front. The energy dissipation across the bore was calculated using equations II.7-II.10. The values on the low side of the bore were determined by the location in the time series just before the bore passed the sensors and the values on the high side of the bore

Table 2.4 R-squared values for observed transport vs. a surrogate Bagnold-type relation

Fluid Forcing	Instantaneous Transport, i r^2	Fluid Forcing	Total Transport, I r^2
Uprush	N=11740	Uprush	N=740
u^2	0.68	$u^2\Delta t$	0.63
u^3	0.64	$u^3\Delta t$	0.59
u^4	0.59	$u^4\Delta t$	0.54
Backwash	N=12660	Backwash	N=740
u^2	0.40	$u^2\Delta t$	0.54
u^3	0.37	$u^3\Delta t$	0.46
u^4	0.34	$u^4\Delta t$	0.41

0.5 seconds after the bore passed the sensors. In order to view the bore as a stationary feature we performed a Galilean transformation on the observed flow velocities by subtracting the bore velocity. This yields a perspective in the frame of reference of the bore itself. The bore velocity, U_b, was obtained by expanding II.7 to its full form

$$(u_1' - U_b)h_1 = (u_2' - U_b)h_2, \tag{II.13}$$

and U_b was obtained by algebraic manipulation of II.13

$$U_b = \frac{u_2'h_2 - u_1'h_1}{h_2 - h_1}. \tag{II.14}$$

Figure 2.20A shows the conservation of momentum results (equation II.8) using U_b as obtained from above. M_1 and M_2 are the momentum fluxes on the low (supercritical) and high (subcritical) sides of the bore respectively. The solid line is the 1-1 line with the dashed line representing the least squares fit to the N=24 data points. Momentum conservation would require the points fall on a 1-1 line, however, momentum is not perfectly conserved from the data. It can be seen that the momentum flux density is consistently greater on the low side of the bore. Although our momentum estimates are not exactly 1-1, the r^2 value was 0.81 at the 99 % significant level with a slope coefficient of roughly 0.66.

The observed difference in the momentum balance was possibly a result of momentum dissipation via shear stress at the bed or the assumption of uniform velocity

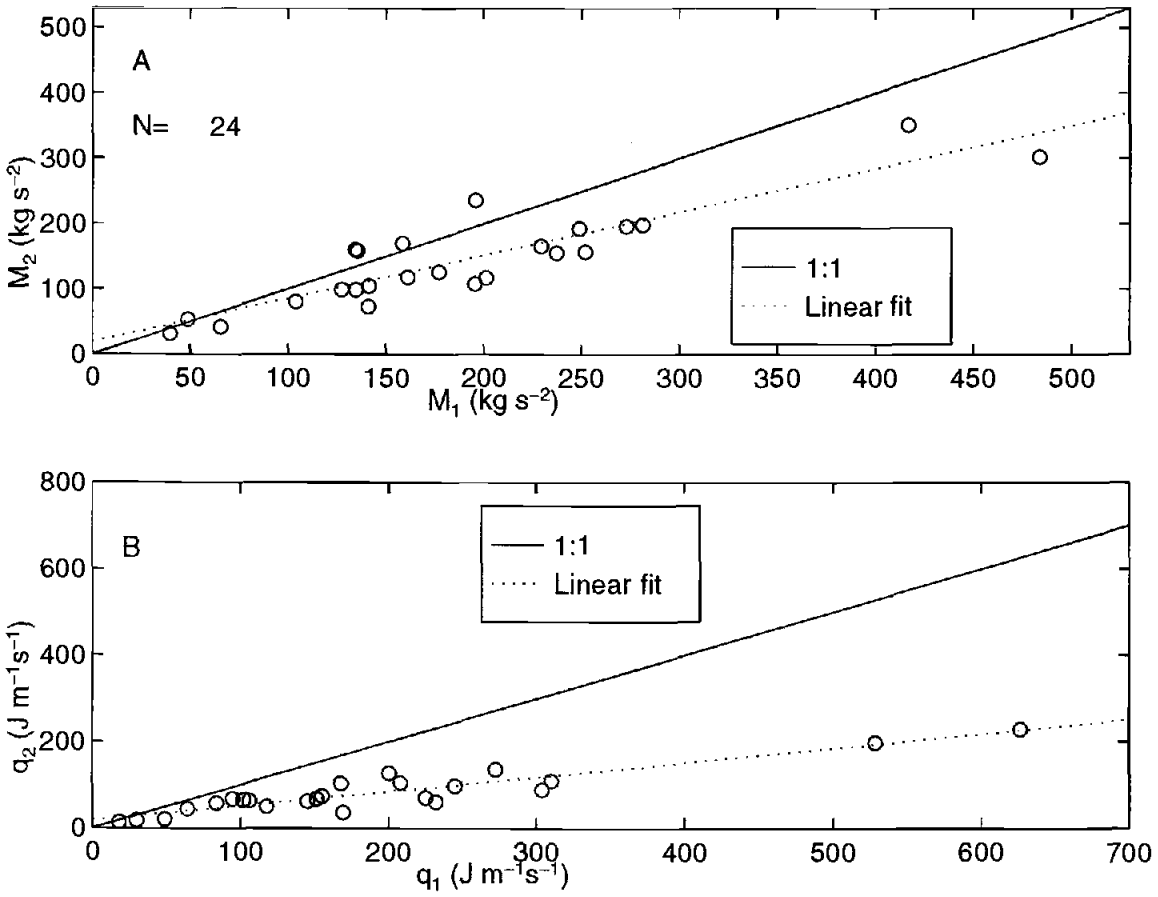

Figure 2.20. A) Momentum flux density on the low (subscript 1) and high side (subscript 2) of a bore for the N=24 bores chosen. The solid line is the 1:1 line and the dotted line is the least squares regression line. The r^2 value was 0.81 at the 99 % significance level with a regression slope of approximately 0.66. B) Energy flux densities on both sides of the bore as explained in A. The r^2 values was 0.85, significant at the 99 % level with a regression slope coefficient of 0.33.

profiles. Figure 2.20B shows the energy flux density across the bore. Since the momentum conservation was not exact, we did not expect II.10 to yield the most appropriate energy dissipation since it was derived from substitution using II.8. Therefore, we estimated the energy dissipation across the bore using II.9. The energy fluxdensity is not constant across the bore and the drop results from the turbulence due to continual bore breaking. The drop in energy was linear in the cases observed with an r^2 value of 0.85 significant at the 99 % level. The slope coefficient was 0.33 indicating that roughly 2/3 of the energy was dissipated across the observed bores. It is this energy dissipation that may be important to local sediment transport processes.

Bagnold's (1963, 1966) energetics arguments showed the fluid power which is proportional to ρu^3, has units of J m^{-2} s^{-1}, where J is joules. This power was related to the immersed weight sediment transport u**C**gs, which has units of J m^{-2} s^{-1}, so that the units are consistent. The energy flux density, q has units of J m^{-1} s^{-1}, and does not carry the same units as the Bagnold-type equation, however, we are interested in using the energy dissipation across the bore (Δx) to relate to the observed sediment transport. Hence from

$$\frac{\partial}{\partial t}E = -\frac{\partial}{\partial x}q, \qquad \text{(II.15)}$$

where E is the energy density. It might be expected that the immersed weight sediment transport is related to the spatial rate of change of the energy flux density since this change in energy flux is the energy available to do work on the sediment. In discretized form,

$$\frac{q_1 - q_2}{\Delta x} \sim u\mathbf{C}gs, \tag{II.16}$$

where ~. implies the two quantities may be related. Rearranging II.16 yields

$$q_1 - q_2 \sim u\mathbf{C}gs\Delta x. \tag{II.17}$$

Equation II.17 was used to compare the energy dissipation across the bore to the spatial scale, Δx, times the immersed weight transport observed on the high side of the bore (Figure 2.21A). The r^2 value for the regression was 0.80 with a significance of 99 %. These results show a relationship existed between the bore generated turbulent dissipation and the suspended sediment transport on the high side of the bore. Figure 2.21B shows the suspended sediment transport plotted against the estimated shear stress calculated from ρu_2^3, for u_2 on the high side of the bore. There is a great deal of scatter with an r^2 value of only 0.17 which implies that the simple estimate of the shear stress does not adequately predict the observed sediment response. An estimate of the mean suspended sediment transport across the bore $[0.5*(u_1\mathbf{C}_1+u_2\mathbf{C}_2)gs]$ times Δx is plotted against the energy dissipation in Figure 2.21C. The r^2 value was the 0.80 at a significance of 99 % similar to Figure 2.21A. Figure 2.21D shows the mean suspended sediment transport across the bore plotted as function of the mean estimated shear stress. The correlation was similar to Figure 2.21B in that it was poor (r^2 was 0.44, significant at the 99 % level).

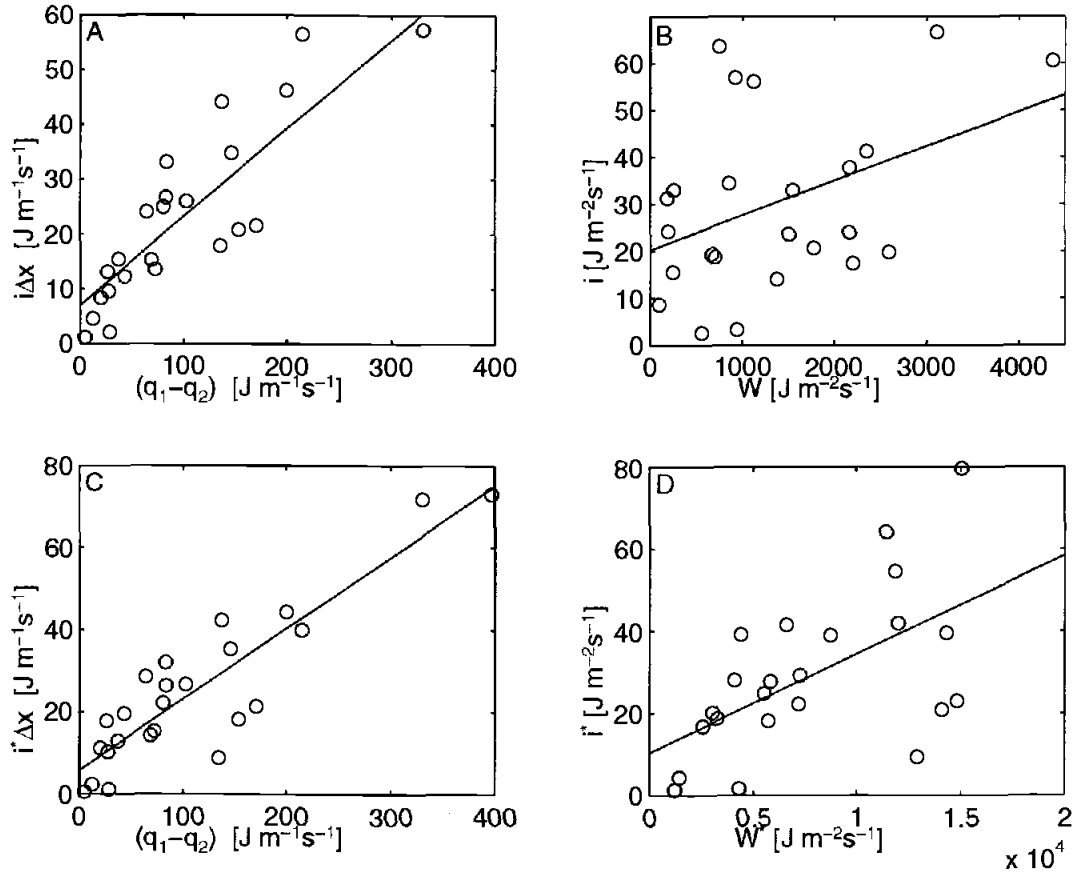

Figure 2.21. A) Linear regression of suspended sediment transport ($i\Delta x$) on the high side of the bore as a function of energy dissipation across the bore (N=24). The r^2 value was 0.80 at a significance level of 99 %. B) The suspended sediment transport (i) plotted against the estimated shear stress (ρu_2^3). The r^2 value was 0.17 at the 99 % significance level. C) Average suspended sediment transport across bore plotted against the energy dissipation. The r^2 value was 0.80 at a significance level of 99 %. D) Average suspended sediment transport across the bore plotted against shear stress estimation from the mean velocity across bore. The r^2 value was 0.44 at a significance level of 99 %.

While the results from Figure 2.21A,C show some scatter about the linear fit, the relationships were much stronger than those for the estimates of the commonly used Bagnold-type formulations.

Alternatively, a dimensional argument can be developed in regards to energy dissipation across the bore. As previously mentioned, the dissipation results in turbulence which may maintain suspension and transport sediment. Hence we may expect a relationship between the time rate of change in energy across the bore, $\partial E/\partial t$, and the time rate of change of the potential energy of the sediment. The depth integrated potential energy of the sediment, PE, is defined as

$$PE = \int_0^h dz \int_0^h \frac{\rho_s - \rho}{\rho_s} g c(z) dz. \tag{II.18}$$

The above arguments simply imply that $\partial PE/\partial t$ is proportional to the total time rate of change of energy across the bore (II.9), or

$$\frac{\partial}{\partial t} PE \propto \frac{\partial}{\partial t} E = -\frac{\partial}{\partial x} q. \tag{II.19}$$

Discretizing II. and rearranging yields

$$q_1 - q_2 \propto \frac{\Delta x}{\Delta t} PE \;\Rightarrow\; q_1 - q_2 \propto U_b PE, \tag{II.20}$$

where, again, we assume $\Delta x=U_b\Delta t$. The relation (II.20) compares the difference in energy fluxes across the bore to an estimate of $PE\Delta x/\Delta t$ which is equivalent to a flux in the potential energy of the sediment at the bore velocity, U_b.

Figure 2.22A shows the calculated U_bPE_2 as a function of the energy dissipation. the circles represent the cases when the momentum flux on the subcritical side of the bore was less than that estimated on the super critical side of the bore (Figure 2.20). The '+' signs are the few cases where the estimated momentum flux was greater on the subcritical side when compared to the super critical side. The linear regression was performed only through the circles in the figure yielding an r^2 value of 0.73 significant at the 99 % level. Similarly, we compared an average estimate for $PE\Delta x/\Delta t$ ($0.5*U_b[PE_2+PE_1]$) to the estimated energy flux difference (Figure 2.22B). Again, the regression was calculated only through the circles in the figure. The r^2 value was 0.72 significant at the 99 % level. This dimensional argument also shows that the energy dissipation across the bore is related to the observed sediment response. Specifically, the bore turbulence (proportional to the energy dissipation) is correlated with the flux of the potential energy of the sediment at the bore velocity.

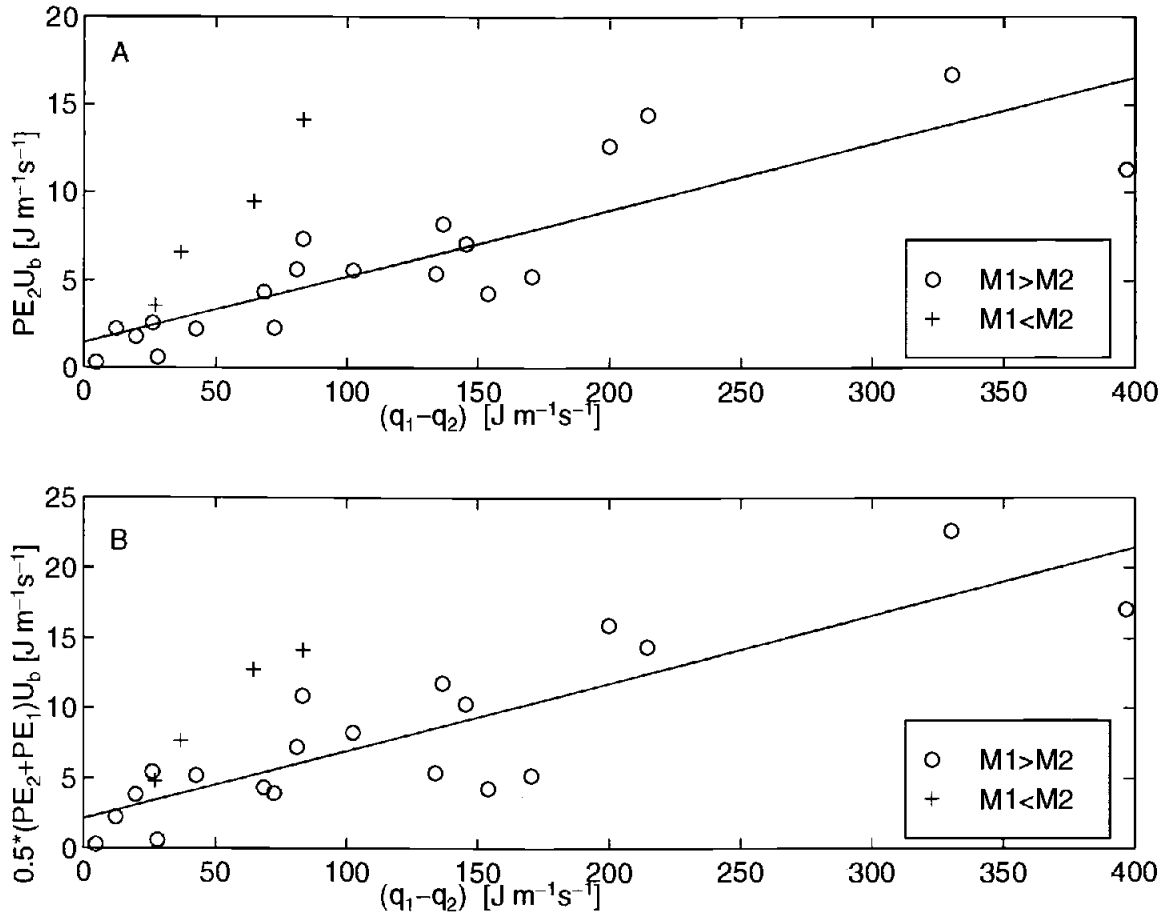

Figure 2.22. A) Linear regression of flux of potential energy of sediment (U_b*PE_2) onto the energy dissipation across the bore (r^2 = 0.73 significant at the 99 % level). B) Mean flux of potential energy of sediment (0.5*U_b[PE_1+PE_2]) regressed onto energy dissipation across bore (r^2 = 0.72 significant at the 99 % level). Regression in both cases was through circles only.

Discussion

Suspended sediment concentrations in the uprush of all three duration ensemble averages were found to be maximum in the leading edge and nearly vertically uniform from above the lower 1-3 cm up to the height of the sensors with maximum values exceeding 80 g l^{-1}. Shortly after sensor inundation by the uprush, the suspended sediment concentration decreased rapidly and little suspended sediment remained in the water column until the backwash began. In all cases, suspended load in the uprush exceeded the suspended load in the backwash (up to a factor of 2). These findings are similar to those of Osborne and Rooker (1997, in review). However, they, found that suspended sediment concentrations increased gradually in the backwash and peaked under the accelerating, thinning flow. The present data show that backwash duration is an important limitation in suspended sediment concentration. The 6 second duration ensemble average event showed very little increase in suspended sediment during the backwash when the thinning flow velocities and accelerations were large. The 9 and 12 second ensemble average events showed a substantial increase in near bed suspended sediment concentration as the backwash had more time to develop. The accelerating, thinning flow gradually suspended sediment, and as the backwash neared its completion, sediment was distributed slightly higher (2-3 cm) into the water column (Figure 2.15A, ~8.75 seconds; Figure 2.16A, ~11.75 seconds) until the water depth pinched to zero. Here, the backwash is analogous to water flowing down an inclined plane. As the water accelerates downslope, the boundary layer thickens allowing turbulent eddies to transport sediment slightly higher into the water column. This process cannot continue, however, as the water depth pinches to zero at the very end of the backwash. Therefore, sediment

suspension in the swash zone, specifically in the backwash, is at least partially controlled by the water depth and duration. Because the initial and final water depths for a swash event were allowed to be less than 10 cm for this analysis, instead of zero for some definitions of the swash zone, the uprush and backwash suspension within the swash zone may have been slightly underestimated.

One of the more important results obtained from the study was the observation of very high SSC signals. Some nearshore and swash zone studies have used only bed load as the sediment transport mechanism (e.g., Turner, 1995; Bailard and Inman, 1981). The present data showed that suspended load transport within the swash zone is significant and excluding the suspended load, as above, will underestimate transport magnitudes.

It was noted by Broome and Komar (1979), that backwash motion down the beach face colliding with an incoming uprush can produce an undular hydraulic jump, which alters the sediment transport. An undular hydraulic jump has an associated high amount of turbulence over a short cross-shore scale. This concentrated turbulence may be the suspending mechanism yielding the large observed suspended loads in the uprush. Furthermore, Brenninkmeyer (1976a,b) observed 'sand fountains' , pulses of high sediment suspension into the water column, occurring in the transition zone between surf and swash (ie; where backwash /uprush collision occurs). He attributed the 'sand fountains' in the transition zone to the formation of a hydraulic jump that may suspend the sediment. If advection of sediment within the swash zone is indeed significant, then hydraulic jumps and backwash/uprush collision may be the important suspending mechanisms feeding the advection process.

Kroon *et al.* (1991) found with pump samplers that the time averaged SSC at several vertical locations within the water column (up to 20 cm) within the swash zone was approximately 10-20 g l^{-1} and nearly vertically uniform. The mean profiles obtained in the present study at the landward and middle locations (up to 12 cm) had values that were 2-3 times those of Kroon's, and were not vertically uniform. Horn and Mason (1994) used a sediment trap and found that bedload transport dominated the backwash while both bedload and suspended load transport were important in the uprush of the four beaches they studied. The device used by Horn and Mason, (1994) sampled bed load up to 1 cm above the bed. The ensemble averages (Figures 2.14A,2.15A and 2.16A) may be consistent in that suspended sediment very close to the bed seemed to dominate the backwash. Furthermore, a comparison with one of the beaches in their study that most closely matches Gleneden in wave energy showed a dominance in suspended load transport in the uprush and bedload transport in the backwash

Beach and Sternberg (1991) found that the incident band energy contribution to net sediment flux in the swash zone was directed primarily onshore, which is consistent with the present findings for the ensemble swash averages. Although much of the swash zone energy was in the infragravity band, net sediment transport at the 3 cross-shore locations was onshore and was consistent with survey data. In another study using FOBS instruments, Beach *et al.*, (1992b) found that SSC's were in excess of 200 g l^{-1} in the swash zone and differed considerably between uprush and backwash. Although the particular FOBS for the present study could not record values that high, the present data

did show that the SSC's could exceed 160 g l^{-1} in the swash and similar to Beach *et al.*, (1992b) showed that the SSC varied considerably from uprush to backwash.

Because the distinction between surf and swash zones may occur in a short cross-shore distance, some of the measurements within this study may have actually been surf zone measurements. For instance, the experiment was conducted over a high tide cycle, causing the seaward sensors to be almost continually submerged and may have been subjected to surf zone processes such as wave breaking. The lack of intermittency in sea surface combined with our definition of swash would imply that the seaward sensors were in the swash zone only 27 to 57 % of the data run. Figure 2.13 showed that the mean suspended sediment profile at the seaward sensors decreased rapidly away from the bed and was very small within the water column. This type of SSC profile may be more indicative of the surf zone where little sediment is suspended above the bed except near the breakpoint. The cross-shore gradients in sediment suspension between the sensors and the amount of time the instruments were in the swash zone according to our definition, suggested that the transition between the inner surf zone and swash zone occurred in a narrow (~5 m) cross-shore distance or about 50 cm vertically on a steep beach such as this.

The present data did not show a strong correlations between the observed sediment transport and a Bagnold-type formulation. It is possible that we have underpredicted the exact relationships by using stepped velocity profiles or saturated FOBS signals to determine the sediment transport. Furthermore, high SSC's moving

down the beach face as a carpet of bedload (sheet-flow conditions) may have been mapped as the bed in our bed finding routine and caused an underestimation of the backwash suspended load. However, the regression slopes obtained for the total suspended load uprush transport when plotted against $\overline{u}^n\Delta t$ for n=2,3 in this study were 2.92 and 2.26 respectively which are very similar to those obtained by Hughes *et al.*, (1997). Although the regression slopes were similar, the r^2 values in the present study were lower. Interestingly, in the Hughes data as well as this data set, the r^2 values were higher for the relationship with n=2. The similarities between their slope coefficients (using total load) and those of the present study (using suspended load) reinforce the importance of the suspended sediment transport in the swash zone.. Furthermore, results of the present data set and our interpretation of the results from prior studies (Hughes *et al.*, 1997 and Hardisty, *et al.*, 1984) have shown that the Bagnold-type formulations may be inadequate for accurately describing swash zone sediment transport.

The observations as well as regression analysis showed a relationship between the leading edge of the uprush (bore) and suspended sediment transport. Madsen and Svendsen (1983) and Svendsen and Madsen(1984) analyzing numerical models stated that the boundary layer will be weak at the bore front and will not be significant until well behind the bore. Furthermore, the turbulence will spread downward from the free surface, and if the water is shallow enough, will interact with the bottom itself. Yeh and Ghazali (1988) reported on turbulence observations from a laboratory study. They found that close to the shore, the turbulence associated with a bore is advected with the bore front and ultimately acts on the dry beach bed, while a relatively calm flow was observed

behind the bore front. The studies of Madsen and Svendsen (1983), Svendsen and Madsen (1984) and Yeh and Ghazali (1988) as well as the present data have shown both qualitatively and quantitatively that bore turbulence is significant near the shoreline and ultimately affects the sediment bed. It seems important, then, that any comparison or prediction of swash zone sediment transport should include bore generated turbulence. Models such as those of Kobayashi *et al.*, (1989), which can predict sea surface elevations and cross-shore velocities from the surf zone into the swash zone would be prime candidates for employing the concepts of bore turbulence and advection, thereby assisting in the prediction of swash zone sediment transport.

Conclusions

A swash zone sediment suspension and transport study was conducted on a steep, high energy Oregon beach. The study showed that the SSC in the uprush was high, nearly vertically uniform above the lower 2-3 cm, and concentrated in the leading edge of the uprush. Suspended sediment concentrations were very small during flow reversals and increased in the backwash but were confined to just above the bed where strong vertical gradients existed. Backwash sediment suspension appeared to be related to backwash duration and the development of a boundary layer. Neither the uprush or backwash transport showed a strong dependence on the velocity cubed. The differences between uprush and backwash sediment transport were most likely a result of different fluid forcing. Specifically, it appeared as though uprush transport was influenced by bore turbulence, a phenomenon not commonly addressed in swash zone sediment transport

models. Advection of sediment also appeared to affect observed suspended sediment concentrations.

The observations imply the following uprush scenario: Sediment is suspended when the bore turbulence is able to reach the bed and maintain the sediment in suspension. As the bore collapses, more sediment may be suspended from the energy expended directly on the beach face. Then as the uprush moves up the beach face, the sediment is advected with the leading edge and settles out under gravity until little sediment is left in suspension near flow reversal.

It follows that bed shear stress, owing to boundary layer development, would not be of primary importance to uprush sediment transport. These concepts of bore generated turbulence and sediment advection in the swash zone are rarely considered when compared to the traditional Bagnold-type formulations (developed for uni-directional river flow). Furthermore, these traditional formulations do not appear to be adequate for describing swash zone sediment transport.

Acknowledgements

The authors would like to thank John Stanley and Steve Azevedo for their data management and computer assistance. Thanks also to Todd Holland, Nathaniel Plant, Paul Komar and the Coastal Imaging Lab for their helpful suggestions. The development of the FOBS and the field study was supported by the National Science Foundation, grant

numbers OCE-9415946 and OCE-9102733. The author was supported by the Office of Naval Research, grant numbers N00014-9411196 and N00014-96-1-0957.

CHAPTER THREE

GENERAL CONCLUSIONS

Sediment suspension, transport and their variations within the swash zone were analyzed. First, we addressed the differences in fluid forcing within the uprush and backwash and how these differences affected transport across the swash zone. Next, we analyzed uprush and backwash transport in relation to flow duration. Finally, we compared Bagnold-type formulations to the observed sediment transport as well as addressing the importance of bore turbulence to swash zone sediment transport.

Because the backwash fluid dynamics are not simply the reverse of the uprush dynamics, the sediment response will also vary between the two. Specifically, uprush suspension was found to be very high and confined to the leading edge where bore generated turbulence might have been an important suspending mechanism. There was very little sediment suspended during flow reversal since there was little flow velocity or turbulence to maintain an appreciable load. Sediment suspension in the backwash was influenced by the flow duration as well as the water depth. The back wash flow is analogous to flow down an inclined plane where the increased flow duration may enable a thicker boundary layer to develop and suspend sediment higher into the water column.

The field data showed that the suspension was markedly different across the swash zone with the most seaward instruments (not often in the swash zone according to our definition) recording much less suspended sediment on the average. The middle

sensors (only 5 m further landward) were in the swash zone much more often and recorded much higher suspended sediment concentrations. The signal difference seen between the two instrument locations implies that the surf/swash transition occurs in a narrow cross-shore region. This transition region has been shown in other experiments to be very important for suspending sediment. Here we presume that the turbulence associated with bore travel and collapse that occurs in this region is important for altering local sediment transport processes.

The use of standard sediment transport formulations with this data set was only partially successful. The standard formulations were originally developed for steady, uni-directional river flow and hence may not accurately describe the processes that are occurring in the swash zone. The energy arguments across a turbulent bore were addressed and related to the observed sediment transport. We conclude that the bore turbulence and associated energy dissipation influence the sediment transport in the swash zone, but cannot fully describe the sediment suspension that was observed across the bore front.

Although exact relationships between flow velocity, water depth, bore turbulence and the resulting sediment transport in the swash zone remain unknown, we are encouraged that this data showed some relationship between the observed sediment suspension and energy dissipation across a bore. Furthermore, it was demonstrated that using a Bagnold-type formulation within the swash, and in general, assuming all of the transport to be bedload might be inaccurate. Further study is needed to better assess the

importance of the relationship between energy dissipation across a bore, sediment suspension and the advection of that sediment through the swash zone.

BIBLIOGRAPHY

Bagnold, R.A. 1963. Mechanics of marine sedimentation. In: M.N. Hill (ed.), The Sea-Ideas and Observations. Wiley, New York. pp. 507-528.

Bagnold, R.A. 1966. An approach to the sediment transport problem from general physics. U.S. Geol. Surv. Prof. Paper, 422-I, p. 37.

Bailard, J.A. and D.L Inman. 1981. An energetics bedload model for a plane sloping beach: local transport. Journal of Geophysical Research, 86:2035-2043.

Beach, R.A., and R.W. Sternberg. 1991. Infragravity driven suspended sediment transport in the swash, inner and outer surf zones. In: N.C. Kraus, K.J. Gingerich, and D.L. Kriebel (eds.), Coastal Sediments '91, ASCE, New York, pp. 114-128.

Beach, R.A., R.W. Sternberg and R. Johnson. 1992a. A fiber optic sensor for monitoring suspended sediment. Marine Geology, 103:513-520.

Beach, R.A. and R.W. Sternberg. 1992b. Suspended sediment transport in the surf zone: response to incident wave and longshore current interaction. Marine Geology, 108:275-294.

Brenninkmeyer, B.M. 1976a. Sand fountains in the surf zone. In Davis, R.A. and R.L. Etherington (eds.), *Beach and Nearshore Sedimentation*. Society of Economic Paleontologists and Mineralogists Special Publication No.24:69-91.

Brenninkmeyer, B.M. 1976b. In situ measurements of rapidly fluctuating high sediment concentrations. Marine Geology, 20(2):117-128.

Broome, R. and P.D. Komar. 1979. Undular hydraulic jumps and the formation of backlash ripples on beaches. Sedimentology, 26:543-559.

Carlson, C.T. 1984. Field studies on run-up on dissipative beaches. *Proceedings*, 19th Conference on Coastal Engineering, ASCE, 399-414.

Emery and Gale, 1951. Swash and swash marks. Transactions American Geophysical Union, 32(1):31-36.

Foster, D.L. 1996. Dynamics if the nearshore wave bottom boundary layer. PhD thesis, Oregon State University. 114 pp.

Guza, R.T. and E.B. Thornton. 1982. Swash Oscillations on a natural beach. Journal of Geophysical Research, 87(C1):483-491.

Hardisty, J., J. Collier and D. Hamilton. 1984. A calibration of the Bagnold beach equation. Marine Geology, 61: 95-101.

Holland, K.T. and R.A. Holman. 1997. Video estimation of foreshore topography using trinocular stereo. Journal of Coastal Research, 13(1):81-87.

Holman, R.A. 1981. Infragravity energy in the surf zone. Journal of Geophysical Research, 86(C7):6442-6450.

Holman, R.A. and A.H. Sallenger, Jr. 1986. High-energy nearshore processes. Transactions American Geophysical Union, 67(49):1365-1369.

Horn, D.P. and T. Mason. 1994. Swash zone sediment transport modes. Marine Geology, 120:309-325.

Hughes, M.G., G. Masselink and R.W. Brander. 1997. Flow velocity and sediment transport in the swash zone of a steep beach. Marine Geology, 138:91-103.

Johnson, R.S. 1997. A Modern Introduction to the Mathematical Theory of Water Waves. Cambridge University Press, Cambridge, UK, p.445.

Kobayashi, N., G.S. DeSilva and K.D. Watson. 1989. Wave transformation and swash oscillation on gentle and steep slopes. Journal of Geophysical Research, 94(C1):951-966.

Kroon, A. 1991. Suspended sediment concentrations in a barred nearshore zone. In: N.C. Kraus, K.J. Gingerich, and D.L. Kriebel (eds.), Coastal Sediments '91, ASCE, New York, pp. 328-341.

Landau, L.D. and E.M. Lifschitz. 1959. *Fluid Mechanics.* Pergamon Press LTD, London, p. 536.

Madsen, P.A. and I.A. Svendsen. 1983. Turbulent bores and hydraulic jumps. Journal of Fluid Mechanics, 129:1-25.

Mase, H. 1988. Spectral characteristics of random wave run-up. Coastal Engineering, 12(2):175-189.

Mase, H. 1995. Frequency down-shift of swash oscillations compared to incident waves. Journal of Hydraulic Research, 33(3):397-411.

Moore, D.S. and G.P. McCabe. 1993. *Introduction to the Practice of Statistics.* W.H. Freeman and Company, USA, p. 854.

Osborne, P.D. and G.A. Rooker. 1997. Surf zone and swash zone sediment dynamics on high energy beaches: West Auckland, New Zealand. Coastal Dynamics '97, 814-823.

Osborne, P.D. and G.A. Rooker. 1998. Sand re-suspension events in a high energy infragravity swash zone. Journal of Coastal Research (in review).

Sellin, R.H.J. 1969. *Flow in Channels*. Macmillan, St. Martin's Press, London.

Seymour, R.J. 1986. Nearshore auto-suspending trubidity flows. Ocean Engineering, 13(5):435-447.

Shih, S.M. and P.D. Komar. 1994. Sediments, beach morphology and sea cliff erosion within an Oregon coast littoral cell. Journal of Coastal Research, 10(1): 144-157.

Smith, J.D. 1978. Measurement of turbulence in ocean boundary layers. In:W, Woodward, C.N.K. Mooers and K. Jensen (eds.), Proc. Working Conf. Current Measurement. Univ. Delaware, Tech Rep. DEL-SG-3-78, pp. 95-128.

Sternberg, R.W., N.C. Shi, and J.P. Downing. 1984. Field investigations of suspended sediment transport in the nearshore zone. *Proceedings*, 19th Conference on Coastal Engineering, ASCE, 1782-1798.

Svendsen, I.A. and P.A. Madsen. 1984. A turbulent bore on a beach. Journal of Fluid Mechanics, 148:73-96.

Waddell, E. 1973. Dynamics of swash and implication to beach response. Coastal Studies Institute, Louisiana State University, tech report No. 139. p.49.

Waddell, E. 1976. Swash-groundwater-beach profile interactions. In: R.A. Davis and R.L. Etherington (eds.), *Beach and Nearshore Sedimentation*. Society of Economic Paleontologists and Mineralogists Special Publication No.24:115-125.

Wilson, K.C. 1987. Analysis of bed load motion at high shear stress. Journal of Hydraulic Engineering, 113(1) :97-103.

Yeh, H.H. and A. Ghazali. 1988. On bore collapse. Journal of Geophysical Research, 93(C6): 6930-6936.

Appendix

APPENDIX

LINEAR REGRESSION METHODS

The method for determining the r^2 and significance values follows (Moore and McCabe, 1993). Linear regression was performed to test the relationship between a response variable (for these purposes, generally sediment transport) and an explanatory variable (for these purposes, generally fluid power or energy dissipation). In performing the linear regression, the sum of the squares of the deviations of the data points from the linear fit in the vertical direction is minimized.

The slope, b, of the regression line is given by

$$b = \frac{\Sigma xy - \frac{1}{n}(\Sigma x)(\Sigma y)}{\Sigma x^2 - \frac{1}{n}(\Sigma x)^2}, \tag{A.1}$$

where x is the explanatory variable, y the response variable and n the number of samples. The sample correlation coefficient, r, measures the strength of the linear association between two measured quantitative variables and is defined as

$$r = \frac{\Sigma xy - \frac{1}{n}(\Sigma x)(\Sigma y)}{(n-1)s_x s_y}, \tag{A.2}$$

where s_x and s_y are the standard deviations of the x and y variables respectively. The r-value may also be obtained from A.1 and A.2 as

$$r = b\frac{s_x}{s_y}. \tag{A.3}$$

The square of the correlation coefficient, r^2, is used more often than r in statistical analysis. The r^2 value, often reported as a percent, is the fraction of the variation in y that is explained by its least squares regression onto x.

In order to verify the calculated r-value, the significance of the correlation can be determined. That is, a sample r has been calculated and one should test the null hypothesis that the true correlation coefficient equals zero against the hypothesis $r>0$ by calculating a T test statistic based on the calculated r-value

$$T = \frac{r\sqrt{n-2}}{\sqrt{1-r^2}}. \tag{A.4}$$

This T value is tested in terms of a random variable t having the t(n-2) distribution, where n-2 is the degrees of freedom (Figure A.1). The P-value, or probability, for the test of the null hypothesis against $r>0$ is $P[T \geq t_\alpha(n-2)]$, where α is the significance level. Therefore, a α level is chosen ($\alpha=.01$) and $t_\alpha(n-2)$ is calculated. If $T<t_\alpha$, then the null hypothesis cannot be rejected and there is no statistical significance (for that chosen α) that the true

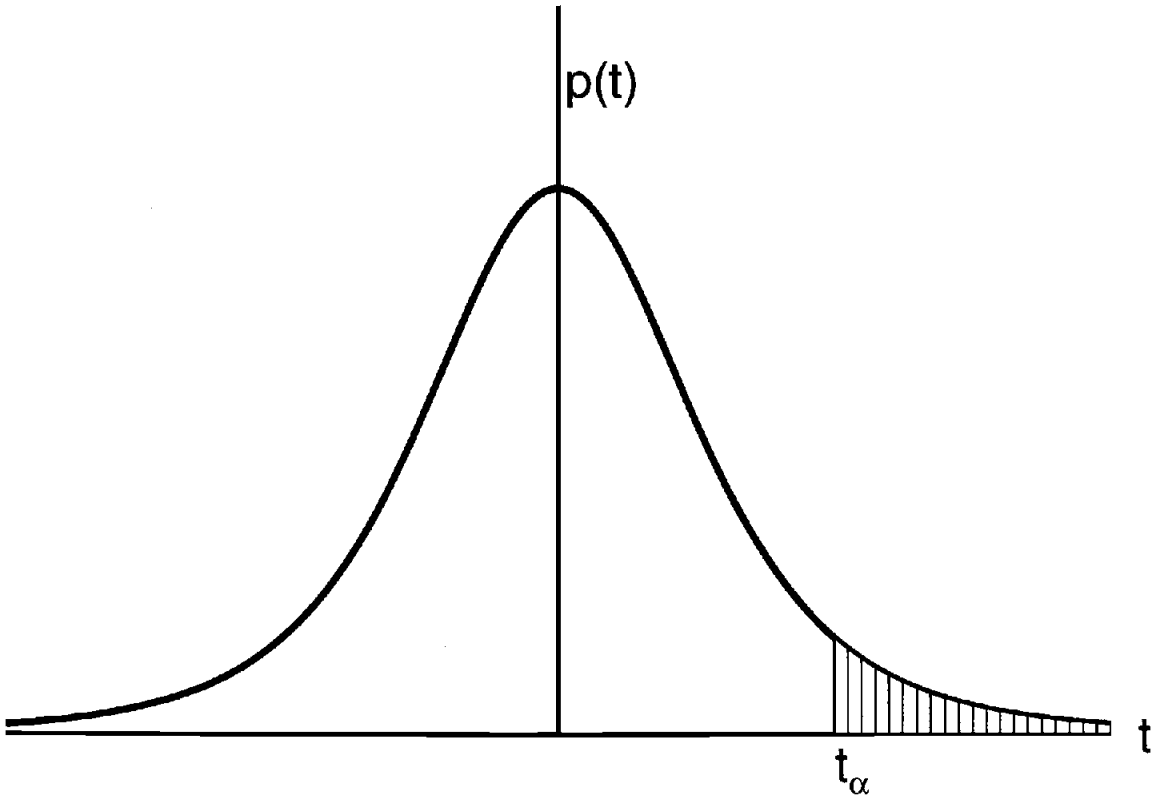

Figure A.1. Diagram of student's t distribution with p(t) represcnting the probability at any given t value. The hashed region represents the area where $T \geq t_\alpha$ at the $100*(1-\alpha)$ significance level.

correlation coefficient is greater than zero. If, however, $T \geq t_{\alpha}$, then the null hypothesis can be rejected and the true correlation coefficient can be accepted as greater than zero with at least the determined statistical significance [$100*(1-\alpha]$).